In: Magnetoresistance
Editor: Russell Gonzalez, pp. 65-121
ISBN: 978-1-53610-598-8


*Chapter 3*

# GIANT INJECTION MAGNETORESISTANCE IN FERROMAGNET/SEMICONDUCTOR HETEROSTRUCTURES

***Leonid Lutsev****
A. F. Ioffe Physical-Technical Institute of the Russian Academy of Sciences, St. Petersburg, Russia

**Abstract**

The giant injection magnetoresistance (IMR) in $SiO_2$(Co)/GaAs heterostructures, where the $SiO_2$(Co) structure is the granular $SiO_2$ film with Co nanoparticles, and in $TiO_2$(Co)/GaAs heterostructures consisting of the amorphous $TiO_2$ film with Co island sublayers is studied. The IMR-effect has positive values, is expressed, when electrons are injected from the granular film into the GaAs semiconductor, and is of the temperature-peak type character. The temperature location of the effect depends on the Co concentration and can be shifted by the applied electrical field. For the $SiO_2$(Co)/GaAs heterostructure with 71 at.% Co the IMR value reaches 1000 ($10^5$ %) at room temperature, which is two-three orders higher than maximum values of GMR in metal magnetic multilayers and TMR in magnetic tunnel junctions. On the contrary, for $SiO_2$(Co)/Si heterostructures magnetoresistance values are very small ($4\%$) and for $SiO_2$(Co) films the intrinsic magnetoresistance is equal to opposite values. High values of the IMR-effect in $SiO_2$(Co)/GaAs heterostructures have been

*E-mail address: l_lutsev@mail.ru

explained by the spin-dependent potential barrier formed in the accumulation electron layer in the semiconductor near the interface. The action of the spin-dependent potential barrier is amplified by the avalanche process in the GaAs and by the electron accumulation in the quantum well in the semiconductor interface region induced by the backscattering process of injected electrons on exchange-splitted levels. The applied magnetic field increases the height and reduces the transparency of the barrier. Efficient magnetic sensors on the basis of ferromagnet / semiconductor heterostructures with holes traps and quantum wells containing spin-dependent potential barrier in the semiconductor at the interface are considered.

**Keywords:** magnetoresistance, semiconductor / granular film heterostructures, cobalt nanoparticles, spin-dependent potential barrier, avalanche process

# 1. Introduction

Magnetic sensors have numerous applications in areas such as position sensing, speed detection, non-contact switching, space exploration, vehicle detection, electronic compasses, geophysical prospecting, non-distructive testing, biomedicine, and brain function mapping [1, 2, 3]. In order to achieve the largest efficiency of magnetic sensors, various effects on the basis of spin-dependent electron transport and magnetoresistance are used.

We consider the magnetoresistance effect in semiconductor / granular film heterostructures with ferromagnetic metal nanoparticles. Since the effect is expressed when electrons are injected from the granular film into the semiconductor, this magnetoresistance effect was called the giant injection magnetoresistance (IMR effect) [4, 5, 6, 7, 8]. For $SiO_2$(Co)/GaAs heterostructures with Co nanoparticles the IMR value reaches 1000 ($10^5$ %) at room temperature, which is two-three orders higher than maximum values of the giant magnetoresistance (GMR) in metal magnetic multilayers and the tunneling magnetoresistance (TMR) in magnetic tunnel junction structures. High values of the IMR effect give us opportunity to use the semiconductor/granular film heterostructures as magnetic sensors with higher sensitivity in comparison with GMR-sensors [9, 10] and as injectors in spin-valve transistors and in spin field-effect transistor structures [11, 12, 13].

Magnetoresistance effects in semiconductor / granular film heterostructures with ferromagnetic metal nanoparticles were studied not long ago. Therefore, there is a small number of papers related to these investigations. Positive huge

magnetoresistance with value of 320000 % in the magnetic field of 2 kOe was observed in semi-insulating GaAs / MnSb island film heterostructures with Sb covers at room temperature [14, 15]. MnSb nanosize islands were the ferromagnetic metal with the Curie temperature of 600 K. The highest value of the magnetoresistance was reached in the avalanche regime. When the deposited atoms formed the uniform MnSb thin film on the GaAs substrate, the huge magnetoresistance effect completely disappeared.

Magnetoresistance effect was studied on heterostructures consisted of semi-insulating GaAs / granular GaAs film with ferromagnetic metal MnAs nanoclusters (shortly, GaAs / GaAs (MnAs)) [16]. The intrinsic magnetoresistance of the GaAs(MnAs) granular film was negative and was equal to 1.5 % in the magnetic field of 10 kOe [17]. On the contrary, the magnetoresistance observed in GaAs / GaAs (MnAs) heterostructures was positive and its value was greater than 600 % in the magnetic field of 10 kOe at room temperature [16]. The magnetoresistance effect was observed in the avalanche regime. The action of the magnetic field led to a suppression of the flowing current.

Positive magnetoresistance of high values was observed in $SiO_2$(Co)/GaAs heterostructures, where the $SiO_2$(Co) was the granular $SiO_2$ film with Co nanoparticles [4, 6, 7]. The IMR value reaches 1000 ($10^5$%) at room temperature. The IMR effect has a temperature-peak type character and its temperature location can be shifted by the applied electrical field. High values of the IMR effect in $SiO_2$(Co)/GaAs heterostructures and the temperature-peak type character are explained by the theoretical model of a magnetic-field-controlled avalanche process provided by electrons passed through the spin-dependent potential barrier in the accumulation layer at the interface [5] and by the spin-dependent current reduction caused by the backscattering process of injected electrons on exchange-splitted levels of the interface quantum well.

High values of magnetoresistance observed in semiconductor / granular film heterostructures with ferromagnetic metal nanoparticles give opportunity to integrate magnetic sensors directly on semiconductor chips. On account of fast avalanche process, magnetic sensors based on the IMR effect can detect high frequency magnetic fields. Thus, one can conclude that IMR-sensors can be used in detection of low-value magnetic fields and of magnetic fields induced by high-speed processes.

In this chapter, we study the magnetoresistance in $SiO_2$(Co)/GaAs, $TiO_2$(Co)/GaAs, and $SiO_2$(Co)/Si heterostructures. Sample preparation and experimental results are presented in section 2. Theoretical model of the IMR-

effect is developed in section 3. The spin-dependent potential barrier is formed by the exchange interaction between electrons in the accumulation electron layer in the semiconductor and $d$-electrons of Co in the interface region. The applied magnetic field increases the height and reduces the transparency of the barrier. The action of the spin-dependent potential barrier on the flowing current is increased by the avalanche process and by the spin-dependent current reduction caused by the backscattering process of injected electrons on exchange-splitted levels of the interface quantum well. High values of the IMR effect in $SiO_2$(Co)/GaAs heterostructures and the temperature-peak type character are explained in section 4. In section 5 we consider ferromagnetic (FM) / semiconductor (SC) heterostructures with holes traps and quantum wells containing spin-polarized localized electrons in the SC at the interface as efficient room-temperature spin injectors and magnetic sensors.

## 2. Sample Preparation and Experimental Results

### 2.1. Sample Preparation

Experiments were performed on samples of amorphous silicon dioxide films containing cobalt nanoparticles grown (1) on gallium arsenide, $(SiO_2)_{100-x}Co_x$/GaAs (or shorter $SiO_2$(Co)/GaAs), (2) on silicon, $(SiO_2)_{100-x}Co_x$/Si (or shorter $SiO_2$(Co)/Si), (3) on quartz substrates, $SiO_2$(Co)/quartz, and (4) on heterostructures $(TiO_2)_{100-x}Co_x$/GaAs (or shorter $TiO_2$(Co)/GaAs) consisting of the amorphous $TiO_2$ film with Co island sublayers on the GaAs substrate [4, 7]. $n$-GaAs substrates with the thickness of 0.4 mm are of the (100)-orientation type. Electrical resistivity of GaAs chips was measured by the dc four-probe method at room temperature and was equal to $0.93{\cdot}10^5$ $\Omega{\cdot}$cm. The 0.4 mm $n$-Si substrates have the orientation of (100) and the resistivity of 3.7 $\Omega{\cdot}$cm. Prior to the deposition process, substrates were polished by a low-energy oxygen ion beam [18, 19]. The roughness height of the polished surfaces did not exceed 0.5 nm.

The $SiO_2$(Co) films were deposited by ion-beam co-sputtering of the composite cobalt-quartz target onto GaAs, Si and quartz substrates heated to 200°C. The concentration of Co nanoparticles in the silicon dioxide deposit was varied by changing the ratio of cobalt and quartz target areas. The film composition was determined by the nuclear physical methods of element analysis using a deuteron beam of the electrostatic accelerator (PNPI, Gatchina, Leningrad re-

gion, Russia). The cobalt to silicon atomic ratio was measured by the Rutherford backscattering spectrometry of deuterons. The oxygen concentration in films was determined by the method of nuclear reaction with deuterons at $E_d$ = 0.9 MeV: $^{16}$O $+d \rightarrow p + {}^{17}$O. This technique is described in more detail elsewhere [20]. For the samples studied, the relative content of cobalt $x$ and the film thickness are listed in Table 1. The average size of Co particles was determined by the small-angle X-ray scattering and increased as the concentration of $x$ grows: from 2.7 nm at $x$ = 38 at.% to 4.4 nm at $x$ = 82 at.%. Cobalt particles are in the ferromagnetic state [21, 22, 23]. The samples with high concentration of Co (71 and 82 at.%) exhibit ferromagnetic behaviour confirmed by the presence of a domain structure (Figure 1) obtained with NT-MDT magnetic field microscope Solver HV-MFM. The period of the domain structure for the $SiO_2$(Co)/GaAs sample with 82 at.% Co is equal to 3.9 $\mu$m, which is smaller than the domain period for the same $SiO_2$(Co) film on the Si substrate (6.0 $\mu$m). The samples with low concentration of Co are superparamagnetic.

The $TiO_2$(Co) films were layer-by-layer grown using the ion-beam sputtering method from the separated $TiO_2$ and Co targets. In contrast to $SiO_2$(Co) films, the granulated $TiO_2$(Co) film has the layered island structure. The first layer deposited on the GaAs substrate was the layer of Co islands. Ten layers of Co islands and ten $TiO_2$ layers were deposited so that the $(Co/TiO_2)_{10}$ structure was formed. The thicknesses of the island layers were identical for all the samples under investigation and were equal to 2.7 nm. The thicknesses of the $TiO_2$ layers were different for the samples under investigation and decreased as the Co content increases. The composition of the films was determined by the neutron activation and X-ray analyses. For the samples under investigation, the Co content $x$ and the total thickness of the $TiO_2$(Co) structure were 34 at. % (45 nm), 55 at. % (40 nm), and 76 at. % (35 nm) (Table 1). For comparison of the characteristics of heterostructures with granulated films, Co films were also deposited on GaAs substrates.

Electrical resistivity of $SiO_2$(Co) films was measured by the dc four-probe method on $SiO_2$(Co)/ quartz heterostructures at room temperature. As the Co content increased, the resistivity of $SiO_2$(Co) films decreased from $1.46 \cdot 10^2$ $\Omega$·cm (38 at.%) to 1.1 $\Omega$·cm (82 at.%).

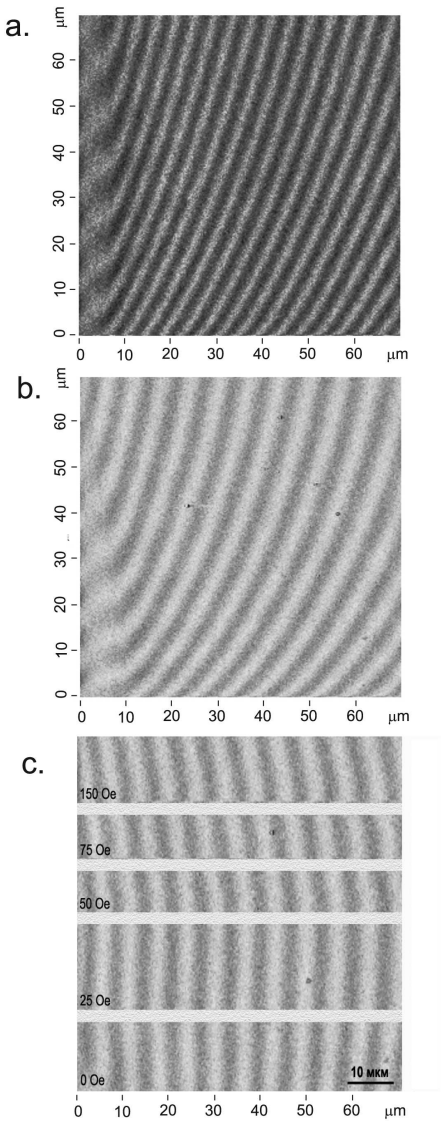


Figure 1. Magnetic field microscope image of the domain structure on samples with $SiO_2$(Co) films with 82 at.% Co (a) on the GaAs substrate and (b) on the Si substrate. (c) Influence of the applied magnetic field on the domain structure on the $SiO_2$(Co)/Si sample with 82 at.% Co.

**Table 1. Properties of $SiO_2$(Co) and $TiO_2$(Co) films sputtered on GaAs, Si and quartz substrates**

| # | **Co concentration** $x$ **(at.%)** | **Thickness** $h$ **(nm)** |
|---|---|---|
| $SiO_2$(Co)/GaAs | | |
| 1 | 38 | 86 |
| 2 | 45 | 81 |
| 3 | 54 | 90 |
| 4 | 71 | 95 |
| 5 | 82 | 95 |
| 6 | 39 | 450 |
| 7 | 60 | 520 |
| 8 | 85 | 600 |
| $SiO_2$(Co)/Si | | |
| 9 | 38 | 86 |
| 10 | 45 | 81 |
| 11 | 54 | 90 |
| 12 | 71 | 95 |
| 13 | 82 | 95 |
| $SiO_2$(Co)/quartz | | |
| 14 | 38 | 860 |
| 15 | 45 | 810 |
| 16 | 54 | 900 |
| 17 | 71 | 950 |
| 18 | 82 | 950 |
| $TiO_2$(Co)/GaAs | | |
| 19 | 34 | 45 |
| 20 | 55 | 40 |
| 21 | 76 | 35 |

## 2.2. Experiment

We have studied the electron transport and magnetoresistance in heterostructures presented in Table 1. Figure 2 shows the current-voltage characteristics for

the $SiO_2$(Co)/GaAs and $TiO_2$(Co)/GaAs structures before the avalanche process in GaAs at room temperature. One contact was on the GaAs substrate, and the other, on the granulated film. The sizes of the samples were equal to $3 \times 3 \times 0.4$ mm. The size of a sample in the current flow direction was equal to 0.4 mm. For $SiO_2$(Co)/GaAs samples with the Co concentration $x$ = 45 - 71 at.%, $TiO_2$(Co)/GaAs samples with the Co concentration $x$ = 55 at.%, and for $SiO_2$(Co)/Si with the Co content $x$ = 38 - 54 at.% the current-voltage dependencies are of the diode type. $SiO_2$(71 at.% Co)/Si structure, $TiO_2$(Co)/GaAs and $SiO_2$(Co)/GaAs structures with low and high Co concentrations (38, 39, 82 and 85 at.% Co for $SiO_2$(Co)/GaAs and 34, 76 at.% Co for $TiO_2$(Co)/GaAs) have nonlinear current-voltage dependencies intermediated between diode and Ohm types. Current-voltage dependencies of $SiO_2$(82 at.% Co)/Si and Co/GaAs are close to the Ohm characteristic. At positive voltages $U$ electrons are injected from the granular film into the semiconductor. For structures of the diode type of the current-voltage characteristic the current density $j$ is high. If the applied voltage $U$ is negative, electrons drift from GaAs to the film and the current density is low. We notice that for $SiO_2$(Co)/GaAs and $TiO_2$(Co)/GaAs samples the resistivity of GaAs is higher than the resistivity of the film and the applied voltage primarily falls on the semiconductor substrate.

The logarithm of the injection current at $U = 35$ V for the $SiO_2$(Co)/GaAs structure (sample #7) with 60 at.% Co and for the $TiO_2$(Co)/GaAs structure (sample #20) with 55 at.% Co is shown in Fig.3 as a function of the inverse temperature $1/T$. The current density $j$ is normalized to the current density $j_R$ measured at room temperature $T = 292$ K. It is seen that the injection current for the $SiO_2$(Co)/GaAs structure is approximated by the law $A_1 \exp(-\varepsilon_1/kT) + A_2 \exp(-\varepsilon_2/kT)$ with the activation energies $\varepsilon_1$ = 0.48 eV and $\varepsilon_2$ = 0.19 eV. The injection current for the $TiO_2$(Co)/GaAs structure is described by the law with the activation energy $\varepsilon$ = 0.071 eV for temperatures near room temperature. For the $SiO_2$(Co)/GaAs structure the temperature dependence is determined by the partial occupied oxygen-ion level $E_1 = 0.48$ eV. The interface region of the GaAs contains oxygen ions leaved after the polished process. According to Refs. [24, 25] in addition to the EL2 defect level, there are oxygen-ion levels in the GaAs bandgap with energies $E_1 = 0.48$ eV, $E_2 = 0.74$ eV, $E_3 = 1.0$ eV, and $E_4 = 1.25$ eV. At room temperature, levels with energies $E_2$, $E_3$ and $E_4$ are occupied by electrons and conductivity is determined by activation of electrons from the level with the energy $E_1$. In Fig.3, for the $SiO_2$(Co)/GaAs structure at the room temperature region the curve $A$ can

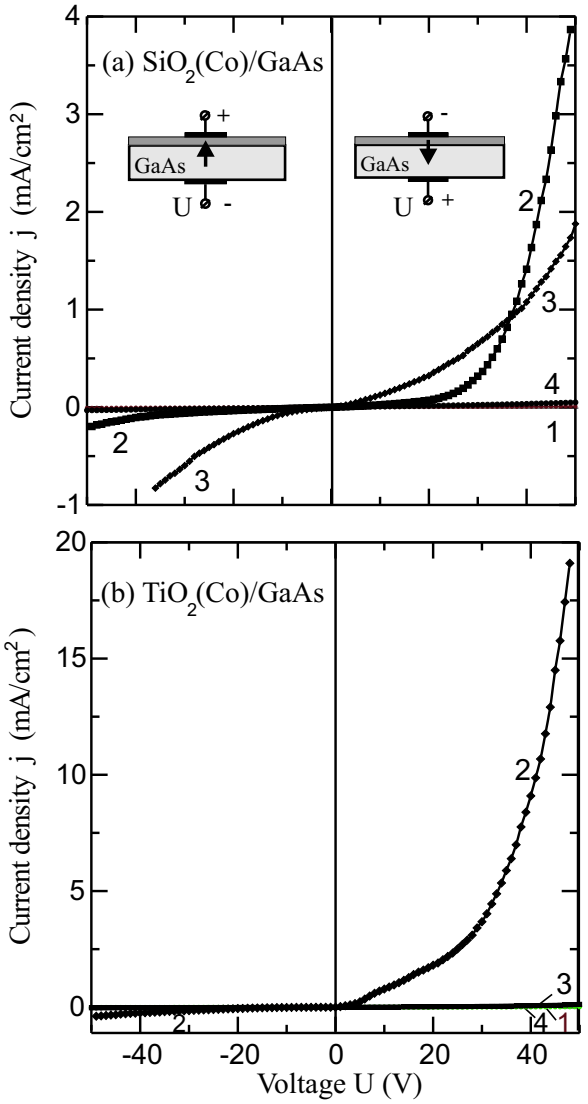


Figure 2. Current-voltage characteristics for (a) the $SiO_2$(Co)/GaAs structure with a Co content of (1) 39 at.%, (2) 60 at.%, (3) 85 at.%, (4) 100 at.% and (b) the $TiO_2$(Co)/GaAs structure with a Co content of (1) 34 at.%, (2) 55 at.%, (3) 76 at.%, (4) 100 at.%.

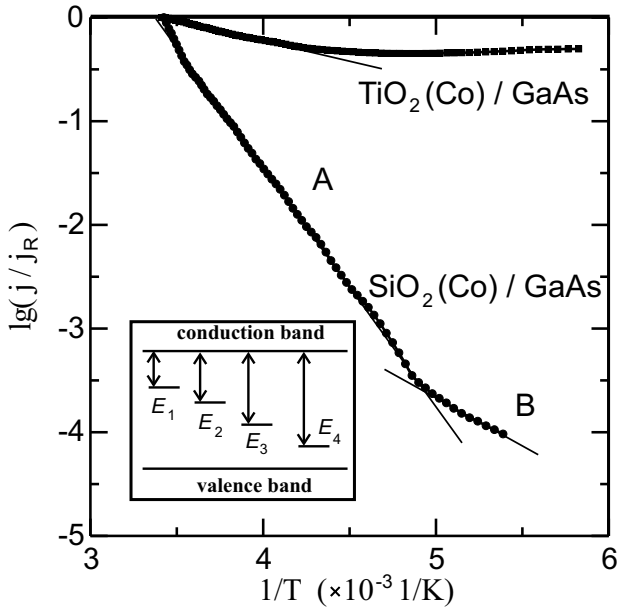


Figure 3. Logarithm of the current ratio $j = j_R$ as a function of reversed temperature for the $SiO_2$(Co)/GaAs heterostructure with 60 at.% Co and for $TiO_2$(Co)/GaAs structure with 55 at.% Co, where $j_R$ is the current at room temperature. Inset shows energy level scheme for the GaAs near the interface.

be approximated by the Arrhenius equation with the activation energy $\varepsilon_1 = E_1$. The current $j$ flowing in the $TiO_2$(Co)/GaAs structure is determined by donors with energy levels $\varepsilon$ =0.071 eV, at the interface GaAs / $TiO_2$(Co).

Figure 4 shows temperature dependencies of the electron inject current density $j$ for the $SiO_2$(Co)/GaAs structure (sample #4) with the Co concentration $x$ = 71 at.% at the applied voltage $U$ = 70 V in the presence of the avalanche process in GaAs. At temperature $T < 300$ K the electron inject current is determined by the electron activation from the energy level $\varepsilon_1 = E_1$ = 0.48 eV. We notice that at the temperature $T$ = 320 K in the absence of a magnetic field the inject current has local minimum. At $T < 320$ K the electron inject current flowing from the granular film into the semiconductor is suppressed by the magnetic field. The magnetic field $H$ is equal to 10 kOe and is parallel to the surface plane of the granular film. At $T > 320$ K temperature dependencies of

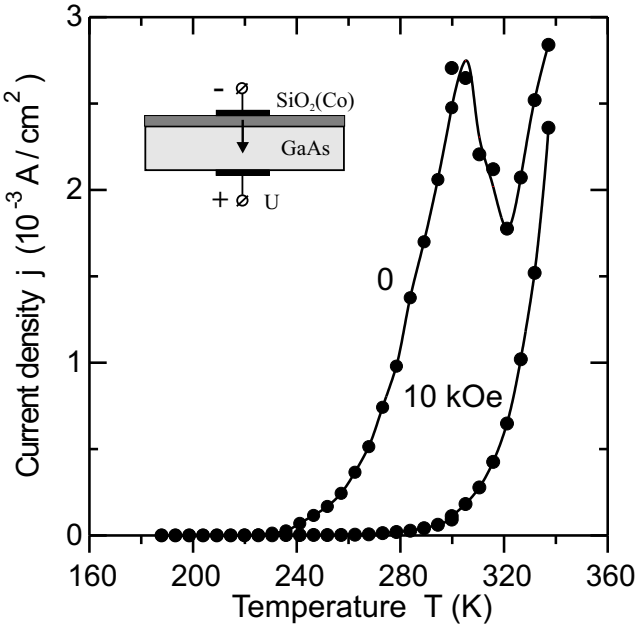


Figure 4. Temperature dependencies of the inject current $j$ for the $SiO_2$(Co)/GaAs structure with the Co concentration 71 at.% at the applied voltage $U$ = 70 V in the absence of a magnetic field and in the magnetic field $H$ = 10 kOe. $H$ is parallel to the surface of the $SiO_2$(Co) film. Solid lines are guides for the eye.

the inject current in the absence of a magnetic field and in the field $H$ are close.

Figure 5 illustrates the effect of the magnetic field on the current-voltage characteristic in the case of the electron injection into the SC for the $SiO_2$(Co)/GaAs structure (sample #4) with 71 at.% Co. For $U > 52$ V, a sharp increase in current due to the process of impact ionization is observed. The applied magnetic field postpones this process to higher electric fields. The magnetic field $H$ is parallel to the film surface. If the magnetic field is perpendicular to the film surface, the dependence of the current on the magnetic field $H$ is weaker because of the demagnetization factor of the film, but the magnetic suppression of the current is still observed.

The relative current density $j(H)/j(0)$ as a function of the magnetic field

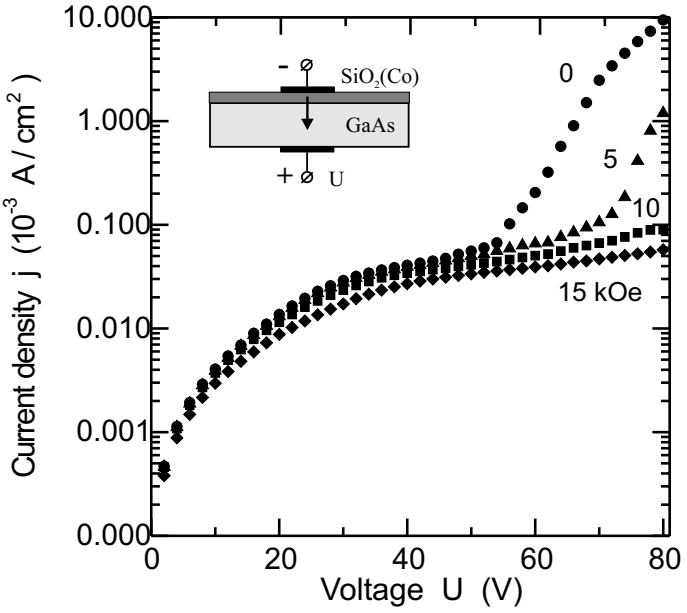


Figure 5. Current-voltage characteristic for the electron injection into the semiconductor for the $SiO_2$(Co)/GaAs structure with 71 at.% Co at different magnetic fields $H$ = 0, 5, 10, 15 kOe. $H$ is parallel to the surface of the $SiO_2$(Co) film.

$H$ for various applied voltages before the avalanche process at room temperature for the $SiO_2$(Co)/GaAs structure with 60 at. % Co (sample #7) is shown in Figure 6. $j(H)$ and $j(0) = j_0$ is the current density in the magnetic field and in the absence of a magnetic field, respectively. At negative voltages, electrons drift from GaAs to the $SiO_2$(Co) film and the effect of the magnetic field on the current is insignificant. At positive voltages, electrons are injected into the GaAs substrate and the current decreases significantly as the magnetic field $H$ increases. If the magnetic field is parallel to the film surface, the injection current $j$ approaches a certain limit as the magnetic field $H$ increases; i.e., saturation is observed. If the magnetic field is perpendicular to the film surface, the dependence of the current on the magnetic field $H$ is weaker and saturation is not observed in the field range 0-23 kOe. Figure 7 shows the relative current density $j/j_0$ as a function of the magnetic field $H$ parallel to the film

for various applied voltages in the $TiO_2$(Co)/GaAs structure with 55 at. % Co (sample #20). The dependence of the injection current on the magnetic field for the $TiO_2$(Co)/GaAs structure is weaker than that for the $SiO_2$(Co)/GaAs one. Compare dependencies presented in Figures 5, 6, and 7, one can conclude that the magnetic field suppresses the injection current at for various applied voltages, but in the presence of the avalanche process in GaAs the suppression is higher.

By analogy with GMR and TMR coefficients [26, 27, 28, 29, 30, 31], we define the injection magnetoresistance coefficient *IMR* as the ratio [4, 6, 5, 7]

$$IMR = \frac{R(H) - R(0)}{R(0)} = \frac{j(0) - j(H)}{j(H)}, \tag{1}$$

where $R(0)$ and $R(H)$ are the resistances of the $SiO_2$(Co)/SC heterostructure without a field and in the magnetic field $H$, respectively; $j(0)$ and $j(H)$ are the current densities flowing in the heterostructure in the absence of a magnetic field and in the field $H$. The *IMR* ratio for the $SiO_2$(Co)/GaAs (samples #6,7,8) and $TiO_2$(Co)/GaAs (samples #19,20,21) structures at the applied voltage $U = 35$ V in the absence of a avalanche process in GaAs is shown in Figure 8 as a function of the magnetic field $H$ parallel to the film. For the $SiO_2$(Co)/GaAs structure with 60 at. % Co, the saturation of *IMR* is observed for high magnetic fields $H$. At the voltage $U = 50$ V in the magnetic field $H = 23$ kOe, the coefficient *IMR* for this structure reaches 52 (5200%). We emphasize that the magnetoresistance effect for single GaAs samples is not observed in such magnetic fields.

The *IMR* ratio at the avalanche process in the GaAs for the $SiO_2$(Co)/GaAs structure (sample #4) with 71 at.% Co at different applied voltages at room temperature (21°C) is shown in Figure 9 as a function of the magnetic field $H$ parallel to the film. The onset of the impact ionization in the GaAs is observed at $U = 52$ V. As seen from Figure 9, the *IMR* coefficient increases with the growth of the applied voltage. At the voltage $U$ = 90 V for this structure the value of *IMR* reaches up to 1000 ($10^5$ %) at room temperature at the field $H$ = 19 kOe. This is two-three orders higher than maximum values of GMR in metal magnetic multilayers and TMR in magnetic tunnel junction structures.

The *IMR* ratio for $SiO_2$(Co)/GaAs structures (samples #1-5) versus the Co concentration $x$ in the in-plane field $H$ = 20 kOe at the applied voltage $U$ = 60 V for different current directions is presented in Figure 10. The *IMR* coefficient has maximum values for structures with Co concentrations in the range [54 - 71 at.%], when electrons are injected from the $SiO_2$(Co) film into the semicon-

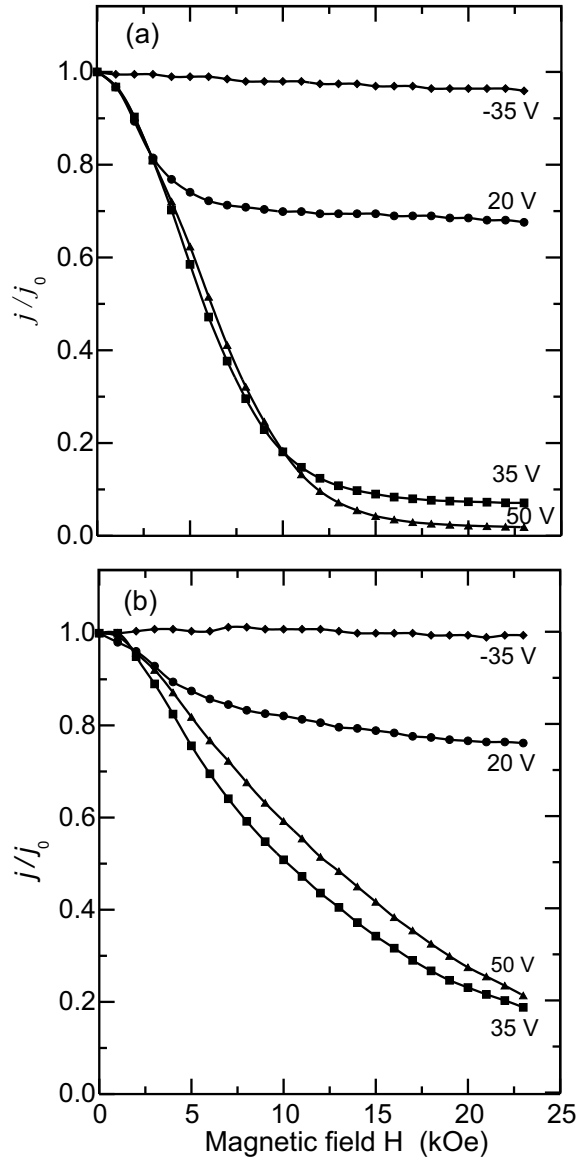


Figure 6. Relative current density $j/j_0$ versus the magnetic field $H$ for various applied voltages for the $SiO_2$(Co)/GaAs structure with 60 at. % Co in the magnetic fields (a) parallel and (b) perpendicular to the film.

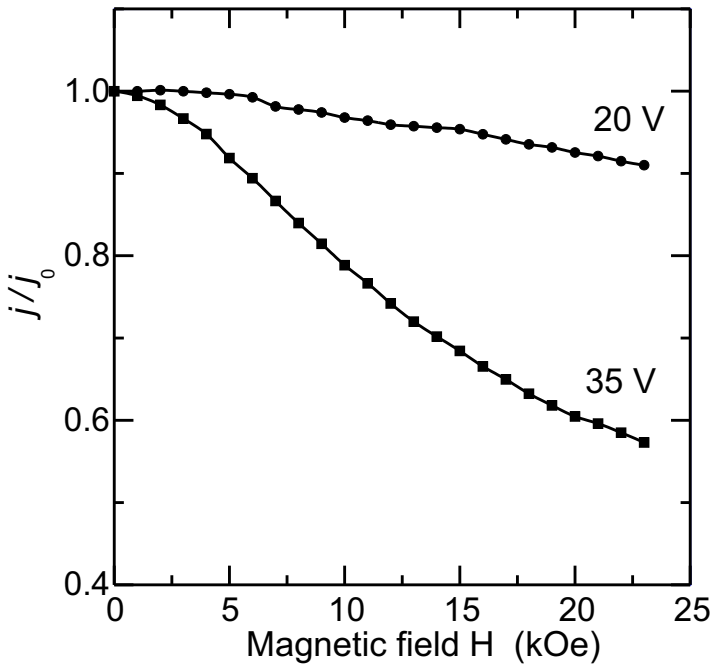


Figure 7. Relative current density $j/j_0$ versus the magnetic field $H$ for various applied voltages for the $TiO_2$(Co)/GaAs structure with 55 at. % Co in the magnetic fields parallel to the film.

ductor. The *IMR* ratio decreases for structures with higher ($x > 71$ at.%) and lower ($x < 54$ at.%) Co concentrations. On the contrary, in the case of the opposite current direction (electrons drift from the semiconductor into the granular film) the magnetoresistance effect becomes less expressed.

As we can see from Figures 8, 9 and 10, for $SiO_2$(Co)/GaAs structures the *IMR* coefficient can reach high values at room temperature. In contrast with this, for $SiO_2$(Co)/Si structures magnetoresistance values are very small and the intrinsic magnetoresistance of $SiO_2$(Co) films has negative values (Figure 11). The magnetoresistance ratio (*MR*) for $SiO_2$(Co) films is determined by the relation analogous to Eq. (1). For $SiO_2$(Co)/Si structures (samples #9-13) electrons are injected from the granular film into the Si substrate. Taking into account low values of the resistivity of Si substrates, experiments were carried out at

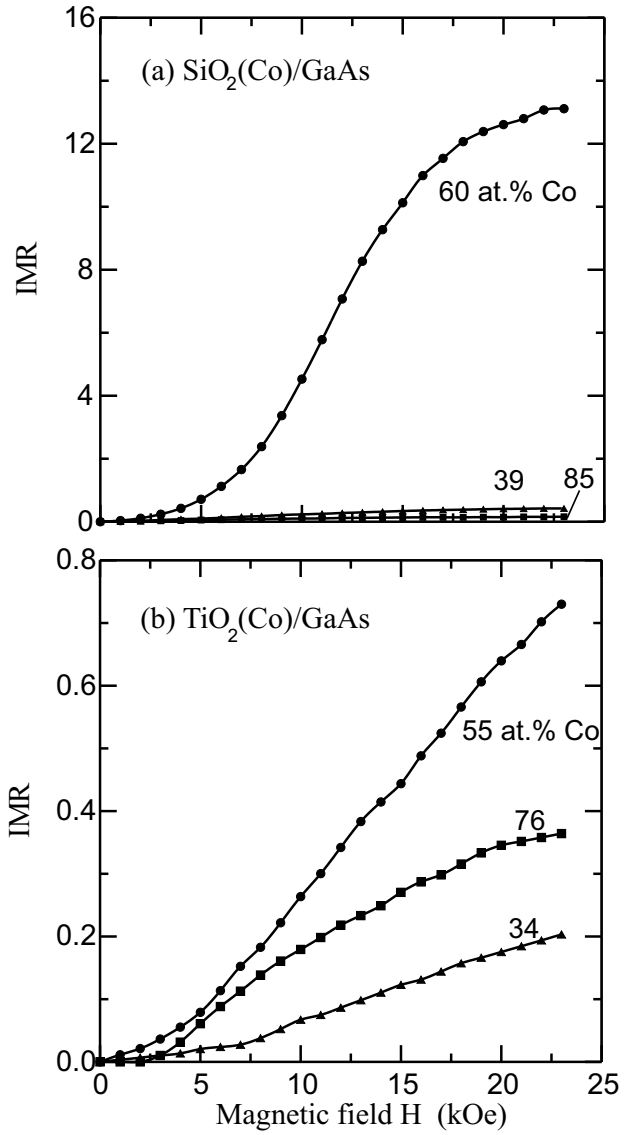


Figure 8. Injection magnetoresistance coefficient *IMR* versus the magnetic field $H$ at the voltage $U = 35$ V for (a) the $SiO_2$(Co)/GaAs structure with a Co content of 39, 60, and 85 at.% and (b) the $TiO_2$(Co)/GaAs structure with a Co content of 34, 55, and 76 at.%. The magnetic field $H$ is parallel to the film plane.

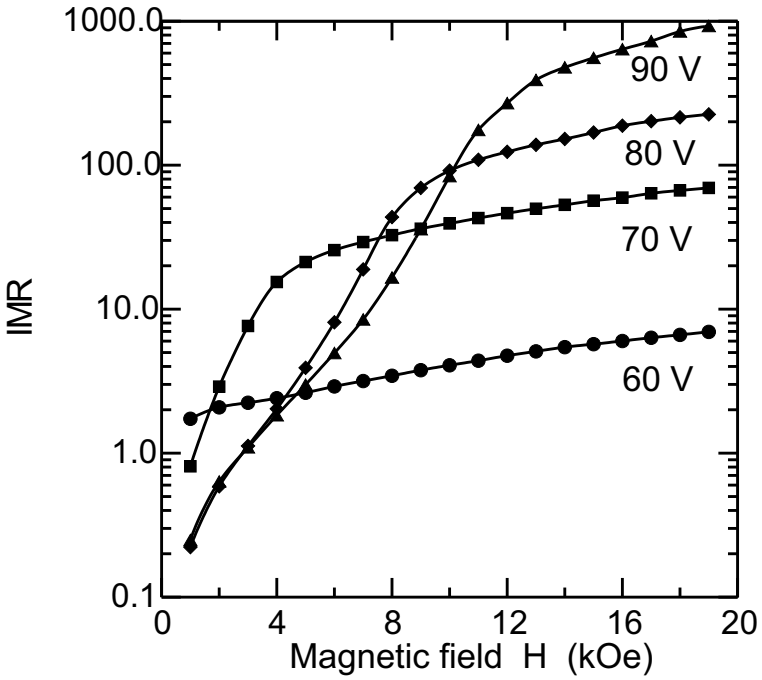


Figure 9. Injection magnetoresistance ratio *IMR* versus the magnetic field $H$ at room temperature for the $SiO_2$(Co)/GaAs structure with 71 at.% Co at applied voltages $U$ = 60, 70, 80, 90 V. $H$ is parallel to the surface of the $SiO_2$(Co) film. Solid lines serve to guide the eye.

the applied voltage $U$ = 3 V. For $SiO_2$(Co) films the intrinsic magnetoresistance ratio was measured by the dc four-probe method on $SiO_2$(Co)/quartz samples (#14-18) in the current-in-plane geometry at the applied voltage $U$ = 60 V at room temperature.

Temperature dependencies of the magnetoresistance can give useful information about the nature of the magnetoresistance effect. Figure 12 presents temperature dependencies of the intrinsic magnetoresistance for $SiO_2$(Co) films with low ($x$ = 38 at.%, sample #14) and high ($x$ = 71 at.%, sample #17) Co concentrations and for the $SiO_2$(Co, 71 at.%)/Si structure (sample #12). Experiments were carried out at the applied voltage $U$ = 60 V for $SiO_2$(Co) films and at $U$ = 3 V for the $SiO_2$(Co)/Si structure. The magnetic field $H$ = 10 kOe is

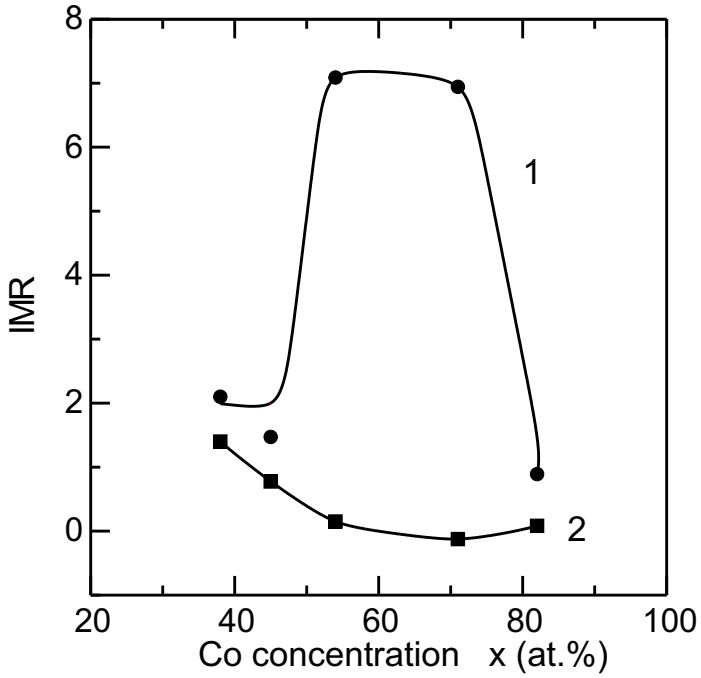


Figure 10. Magnetoresistance ratio *IMR* versus the Co concentration $x$ for $SiO_2$(Co)/GaAs structures in the field $H$ = 20 kOe at the applied voltage $U$ = 60 V for different current directions. (1) Electrons are injected from the $SiO_2$(Co) film into GaAs, (2) electrons drift from GaAs into the granular film. $H$ is parallel to the surface of the $SiO_2$(Co) film. Solid lines serve to guide the eye.

parallel to the surface of the granular film. It can be seen that temperature decreasing causes to the growth of the absolute value of the intrinsic magnetoresistance for $SiO_2$(Co) films. For the $SiO_2$(Co)/Si structure electrons are injected from the granular film into the semiconductor and temperature decreasing leads to the change of the magnetoresistance sign.

Temperature dependencies of the *IMR* for $SiO_2$(Co)/GaAs structures essentially differ from the above-mentioned dependencies for $SiO_2$(Co)/GaAs structures and $SiO_2$(Co) films. They have a peak type character (Figures 13 and 14). The temperature location of the peak depends on the Co concentration

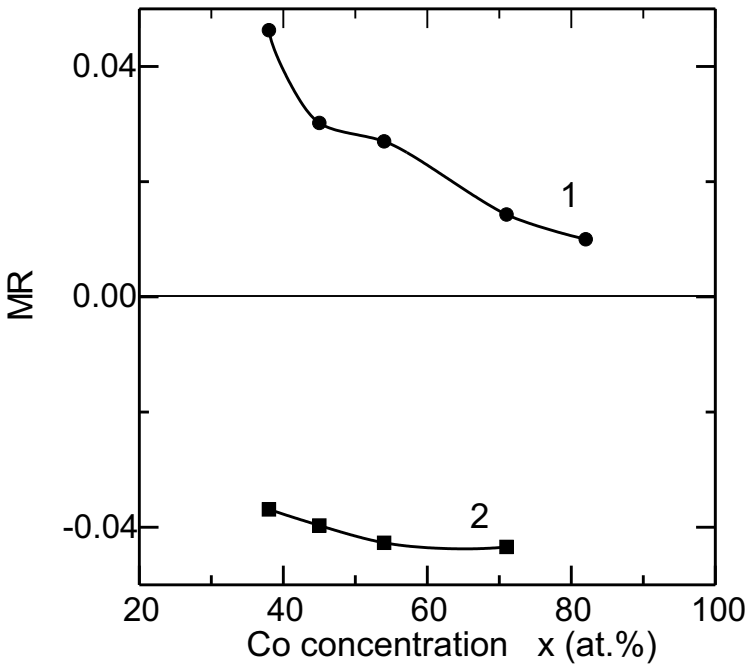


Figure 11. Magnetoresistance ratio *MR* versus the Co concentration $x$ for (1) $SiO_2$(Co)/Si structures and for (2) $SiO_2$(Co) films in the in-plane magnetic field $H$ = 20 kOe. Solid lines serve to guide the eye.

and can be shifted by the applied electrical field. Figure 13 shows temperature dependencies of the *IMR* for $SiO_2$(Co)/GaAs with 71 at.% Co (sample #4) at different applied voltages, when electrons are injected from the granular film into the GaAs substrate. Increasing voltage $U$ causes to a shift of the peak to higher temperatures. At the same time, the voltage growth leads to an increase of the peak magnitude. For $SiO_2$(Co)/GaAs structure with lower Co content ($x$ = 38 at.%, sample #1, Figure 14), the temperature peak of the *IMR* has higher value of width. For the case, when electrons move from GaAs into the $SiO_2$(Co) film, the *IMR* peak is located at higher temperature and its magnitude is lower.

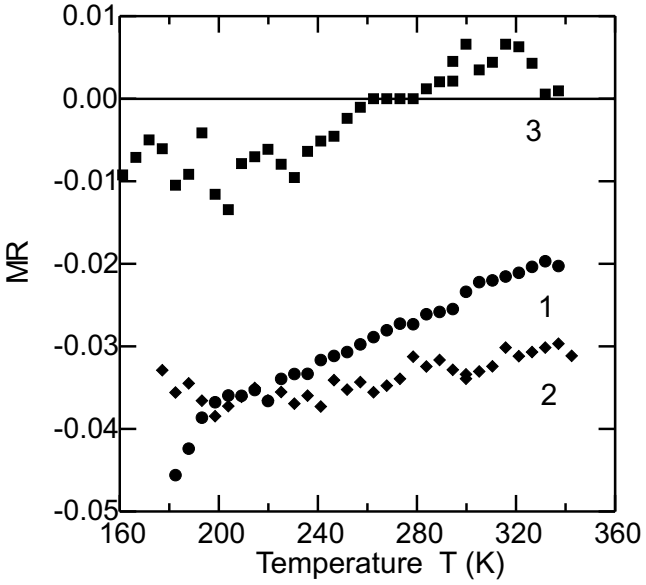


Figure 12. Temperature dependencies of the magnetoresistance *MR* for $SiO_2$(Co) films (1) with $x$ = 38 at.% Co, (2) with $x$ = 71 at.% Co, and (3) for the $SiO_2$(Co)/Si structure with $x$ = 71 at.% Co content in the in-plane magnetic field $H$ = 10 kOe.

## 3. Theoretical Model

Explanation of the IMR effect is based on the spin-dependent potential barrier in the accumulation layer in the semiconductor (SC) at the interface. The applied magnetic field controls the height of the potential barrier, changes the flowing current and results in the IMR effect. Two factors enhance this magnetoresistance effect: (1) the avalanche process in the semiconductor and (2) the backscattering process of injected electrons on exchange-splitted levels of quantum well (QW) in the SC interface region.

In the avalanche process the impact ionization induced by electrons produces holes, which move and are accumulated in the region of the potential barrier. Existence of holes in this region lowers the barrier height. This leads to the growth of the electron current flowing through the barrier. The electron

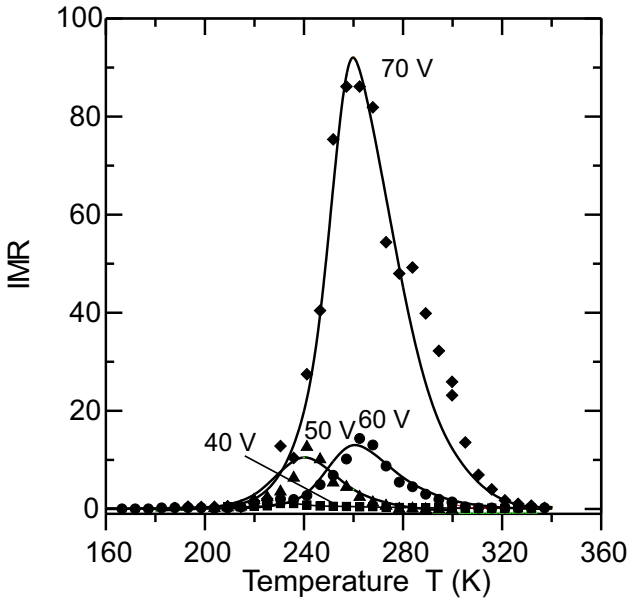


Figure 13. Temperature dependencies of the injection magnetoresistance *IMR* for the $SiO_2$(Co)/GaAs structure with $x$ = 71 at.% Co content in the in-plane magnetic field $H$ = 10 kOe at applied voltages $U$ = 40, 50, 60, 70 V. Solid lines are theoretical fittings.

current growth results in increasing hole concentration in the barrier region and so on. Due to the formed positive feedback small variations in the height of the potential barrier lead to great changes in the flowing current. The electron current growth is accompanied by the appearance of a layer with strong electrical field in the vicinity of the barrier. The change in the electrical field decreases the value of the threshold of the avalanche process making this process more easier in the strong-field layer. The applied magnetic field reduces the transparency of the spin-dependent potential barrier. This decreases the kinetic energy of injected electrons, suppresses the impact ionization onset and reduces the hole concentration.

The backscattering of injected electrons on exchange-splitted levels of the QW results in accumulation of electrons in the QW and leads to the current reduction depended on spins. This results in significant amplification of the

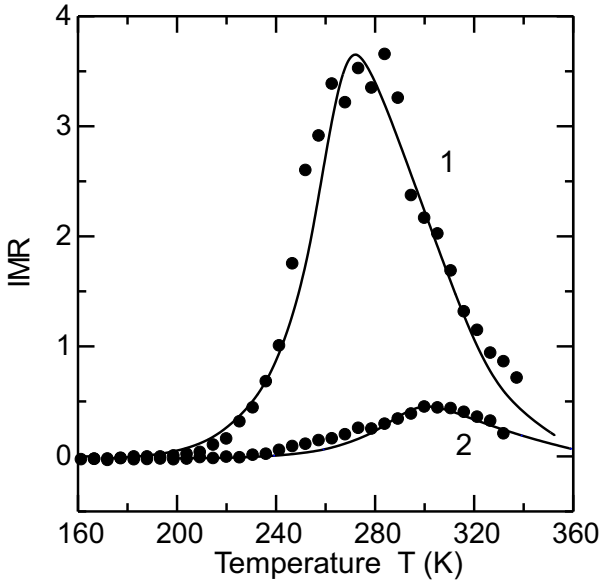


Figure 14. Temperature dependencies of the magnetoresistance *IMR* for the $SiO_2$(Co)/GaAs structure with $x$ = 38 at.% Co content in the in-plane magnetic field $H$ = 10 kOe at the applied voltage $U$ = 60 V. (1) Electrons are injected from the $SiO_2$(Co) film into GaAs, (2) electrons drift from GaAs into the granular film. Solid lines are theoretical fittings.

magnetoresistance effect.

Let us consider formation of the accumulation electron layer in the SC at the interface, the spin-dependent potential barrier, the electrical field distribution, the backscattering and avalanche processes, and the IMR effect caused by the barrier [5, 7].

### 3.1. Hamiltonian

In the ferromagnetic (FM)/SC heterostructure the difference of chemical potentials $\Delta\mu$ between the FM and the SC determines bending of the SC conduction band (Figure 15). $d$-electrons in the FM at the interface and electrons in the accumulation electron layer in the SC are coupled by the exchange interaction $J_0(\vec{r}-\vec{R})$, where $\vec{r}$ is the electron coordinate in the SC and $\vec{R}$ is the coordinate

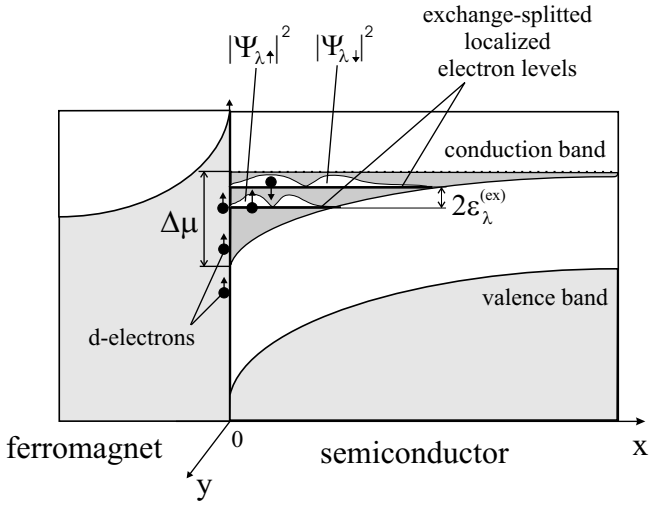


Figure 15. Electronic energy band structure at the contact region of the ferromagnet / semiconductor.

of the $d$-electron in the FM. The Hamiltonian of the model is written in the form

$$\mathcal{H} = \mathcal{H}_e + \mathcal{H}_{ed} + \mathcal{H}_\varphi + \mathcal{H}_s,$$

where

$$\mathcal{H}_e = \sum_\alpha \int \Psi_\alpha^+(\vec{r}) \left[ -\frac{\hbar^2}{2m}\Delta - \mu - e\varphi(\vec{r}) \right] \Psi_\alpha(\vec{r})\, d\vec{r}$$

is the Hamiltonian of electrons with the mass $m$ and the charge $e$ in the SC in the electrical field with the potential $\varphi(\vec{r})$. $\mu$ is the chemical potential. $\Psi_\alpha^+(\vec{r}) = \sum_\lambda \psi_\lambda^*(\vec{r}) a_{\lambda\alpha}^+$, $\Psi_\alpha(\vec{r}) = \sum_\lambda \psi_\lambda(\vec{r}) a_{\lambda\alpha}$ are the second-quantized wavefunctions of an electron with a spin $\alpha = \uparrow, \downarrow$. $a_{\lambda\alpha}^+$, $a_{\lambda\alpha}$ are the creation and annihilation Fermi operators, respectively, for an electron with the wavefunction $\psi_\lambda(\vec{r})$ with the multiindex $\lambda$.

$$\mathcal{H}_{ed} = -\sum_{\vec{R}} \int J_0(\vec{r} - \vec{R})(\vec{S}(\vec{R}), \vec{\sigma}(\vec{r}))\, d\vec{r}$$

is the exchange interaction Hamiltonian between the spin density $\vec{\sigma}(\vec{r})$ of electrons in the SC and spins $\vec{S}(\vec{R})$ of $d$-electrons in the FM. The vector spin density

operator $\vec{\sigma}(\vec{r})$ is determined by operators $\Psi_\alpha(\vec{r})$, $\Psi^+_\alpha(\vec{r})$

$$\sigma_x(\vec{r}) = \Psi^+_\uparrow(\vec{r})\Psi_\downarrow(\vec{r}) + \Psi^+_\downarrow(\vec{r})\Psi_\uparrow(\vec{r})$$

$$\sigma_y(\vec{r}) = -i\Psi^+_\uparrow(\vec{r})\Psi_\downarrow(\vec{r}) + i\Psi^+_\downarrow(\vec{r})\Psi_\uparrow(\vec{r})$$

$$\sigma_z(\vec{r}) = \Psi^+_\uparrow(\vec{r})\Psi_\uparrow(\vec{r}) - \Psi^+_\downarrow(\vec{r})\Psi_\downarrow(\vec{r}).$$

The Hamiltonian

$$\mathcal{H}_\varphi = -\frac{1}{8\pi}\int [\nabla\varphi(\vec{r})]^2\, d\vec{r}$$

describes the classical inner electrostatic field $\varphi(\vec{r})$.

$\mathcal{H}_s$ is the Hamiltonian described the interaction between spins $\vec{\sigma}(\vec{r})$, $\vec{S}(\vec{r})$ and the magnetic field $\vec{H}$

$$\mathcal{H}_s = -g\mu_B\sum_{\vec{R}}(\vec{H},\vec{S}(\vec{r})) - g\mu_B\int(\vec{H},\vec{\sigma}(\vec{r}))\, d\vec{r},$$

where $g$ and $\mu_B$ are the Landé factor and the Bohr magneton, respectively.

In order to find the effective exchange interaction between spins $\vec{S}(\vec{R})$ of $d$ electrons in the FM and the spin $\vec{\sigma}^{(in)}(\vec{r})$ of an injected electron with the wavefunction $\psi^{(in)}_\alpha(\vec{r})$ ($\alpha = \uparrow, \downarrow$) and the spin-dependent potential barrier, the temperature diagram technique is used [32, 33]. Before this we consider formation of the accumulation electron layer.

## 3.2. Formation of the Accumulation Electron Layer

In the self-consistent-field approximation of the diagram expansion electrons of the conduction band in the SC and the inner self-consistent electrical field are described by the following equations.

(1) In the assumption that electrons move freely in the interface ($yz$) plane, equation for the electron wavefunction in the SC along the normal to the interface ($x$-axis) is given by

$$\left[-\frac{\hbar^2}{2m}\frac{d^2}{dx^2} - e\varphi(x)\right]\chi_\nu(x) = \varepsilon^{(0)}_\nu\chi_\nu(x), \tag{2}$$

where $\psi_\lambda(\vec{r}) = V^{-1/2}\chi_\nu(x)\exp(iq_y y + iq_z z)$ is the electron wavefunction in the volume $V$ of the SC with the multiindex $\lambda = (\nu, q_y, q_z)$ and the energy spectrum $\varepsilon_\lambda = \varepsilon^{(0)}_\nu + \hbar^2(q_y^2 + q_z^2)/2m$.

(2) Equation for the inner self-consistent electrical field

$$\Delta\varphi(\vec{r}) = 4\pi e \left\{ \sum_{\lambda,\omega_n} [G_{\lambda\uparrow\uparrow}(\vec{r},\vec{r},\omega_n) + G_{\lambda\downarrow\downarrow}(\vec{r},\vec{r},\omega_n) - G^{(0)}_{\lambda\uparrow\uparrow}(\vec{r},\vec{r},\omega_n) - G^{(0)}_{\lambda\downarrow\downarrow}(\vec{r},\vec{r},\omega_n)] \right\}, \tag{3}$$

where

$$G_{\lambda\alpha_1\alpha_2}(\vec{r}_1,\vec{r}_2,\omega_n) = \frac{\psi^*_\lambda(\vec{r}_1)\psi_\lambda(\vec{r}_2)\delta_{\alpha_1\alpha_2}}{\beta(i\hbar\omega_n - E_{\lambda\alpha_1} + \mu)}, \tag{4}$$

are electron Green functions (Figure 16(a)), $\beta = 1/kT$, $k$ is the Boltzmann constant, $T$ is the temperature, $\hbar\omega_n = (2n+1)\pi/\beta$, $n$ is an integer,

$$E_{\lambda\alpha} = \varepsilon_\lambda \mp \varepsilon^{(\mathrm{ex})}_\lambda. \tag{5}$$

The upper sign in equation (5) corresponds to $\alpha = \uparrow$; the lower sign, to $\alpha = \downarrow$. The energy $\varepsilon^{(\mathrm{ex})}_\lambda$ is determined by the exchange Hamiltonian $\mathcal{H}_{ed}$ in the self-consistent-field approximation

$$\varepsilon^{(\mathrm{ex})}_\lambda = -\sum_{\vec{R}} \int J_0(\vec{r}-\vec{R})(\langle\vec{S}(\vec{R})\rangle_0, \langle\vec{\sigma}(\vec{r})\rangle_0)\, d\vec{r}. \tag{6}$$

$\langle\vec{S}(\vec{R})\rangle_0$ and $\langle\vec{\sigma}(\vec{r})\rangle_0$ are the statistical-average $d$-electron spin in the FM and the electron spin density in the SC, respectively. $G^{(0)}_{\lambda\alpha\alpha}$ are electron Green functions determined in the single SC in the absence of the electrical field.

(3) Relationship between the chemical potential $\mu$ and the electron concentration $n_0$ in the single SC

$$n_0 = \frac{8\pi e}{V} \sum_{\vec{q}=(q_x,q_y,q_z)} n_F[\beta(\hbar^2|\vec{q}|^2/2m - \mu)]. \tag{7}$$

where $n_F(a) = [\exp(a)+1]^{-1}$.

Equations (2), (3), (7) are simultaneous equations in unknowns: the wave function $\chi_\nu(x)$, the energy $\varepsilon^{(0)}_\nu$, the electrical potential $\varphi(x)$, and the chemical potential $\mu$ in the SC. Taking into account that at the interface of the heterostructure ($x = 0$) the potential $\varphi(x)$ is determined by the difference of chemical potentials $\Delta\mu$ between the SC and the FM, $\varphi(0) = \Delta\mu/e$, and at a great distance from the interface, when $x \to \infty$, the potential $\varphi(x)$ tends to zero, we numerically can solve equations (2), (3), (7).

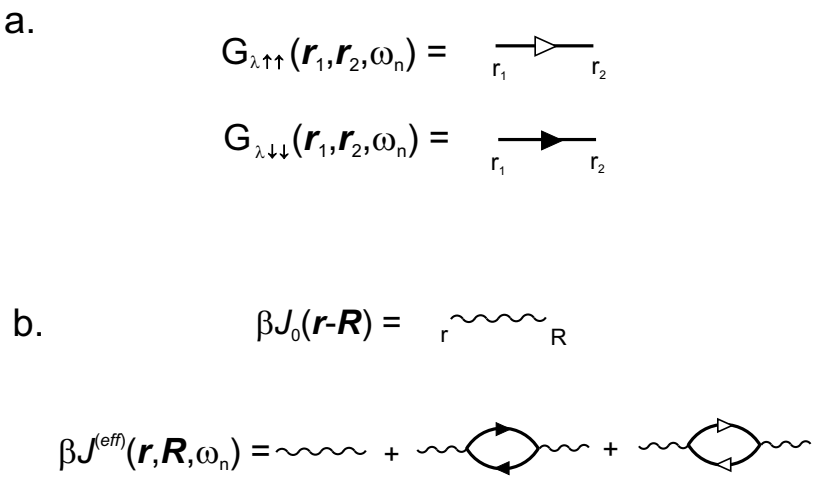


Figure 16. (a) Temperature electron Green functions with the spin $\uparrow$ and $\downarrow$. (b) Bare and effective exchange interactions.

### 3.3. The Effective Exchange Interaction and the Spin-Dependent Potential Barrier

The effective exchange interaction and the spin-dependent potential barrier for injected electrons are found in the next approximation of the diagram expansion. This is the one-loop approximation with respect to the bare exchange interaction $J_0(\vec{r}-\vec{R})$ (figure 16(b)). In this approximation we take into account solutions of equations (2), (3), (7) made in the self-consistent-field approximation and find the effective exchange interaction

$$J^{(\mathrm{eff})}(\vec{r},\vec{R},\omega_n) = J_0(\vec{r}-\vec{R}) + J_1(\vec{r},\vec{R},\omega_n),$$

where the interaction $J_1$ has the form

$$J_1(\vec{r},\vec{R},\omega_n) = -\beta \int\int J_0(\vec{r}-\vec{r}_1)$$

$$\times \sum_{k,\lambda_1,\lambda_2} [G_{\lambda_1\uparrow\uparrow}(\vec{r}_1,\vec{r}_2,\omega_k) G_{\lambda_2\uparrow\uparrow}(\vec{r}_1,\vec{r}_2,\omega_k+\omega_n)$$

$$+ G_{\lambda_1\downarrow\downarrow}(\vec{r}_1,\vec{r}_2,\omega_k) G_{\lambda_2\downarrow\downarrow}(\vec{r}_1,\vec{r}_2,\omega_k+\omega_n)]$$

$$\times J_0(\vec{r}_2 - \vec{R})\, d\vec{r}_1 d\vec{r}_2. \tag{8}$$

In the relation (8) the Green functions $G_{\lambda\alpha_1\alpha_2}$ (4) are expressed via wavefunctions $\psi_\lambda(\vec{r})$, the chemical potential $\mu$ and the electron energy $E_{\lambda\alpha}$ (5). The interaction $J_1$ is of the RKKY-type (Ruderman, Kittel, Kasuya, Yosida [34, 35, 36]). Spins of electrons in the accumulation layer shield spins of $d$-electrons in the FM at the interface. As the result of this shielding, the short-range exchange interaction $J_0(\vec{r} - \vec{R})$ is transformed into the long-range effective exchange interaction $J^{(\mathrm{eff})}(\vec{r}, \vec{R}, \omega_n)$, which changes its sign at a some distance from the interface (figure 17). To find the numerical solution, we assume that $J_0(\vec{r} - \vec{R}) = J_0 \exp(-\xi|\vec{r} - \vec{R}|)$ in equations (6), (8), where $\xi$ is the reciprocal radius of the exchange interaction and $J_0$ is determined by the Coulomb interaction with $d$-electrons on a FM atom [37]. Calculations have been drawn, when $\omega_n = 0$, $\vec{R} = 0$, $\xi$ = 10 nm$^{-1}$, $J_0$ = 2 eV, $|\langle\vec{S}(\vec{R})\rangle_0| = 1/2$, $|\langle\vec{\sigma}(\vec{r})\rangle_0| = 1/2|\psi_\lambda(\vec{r})|^2$, $\Delta\mu$ = 150 meV, $n_0$ = $1\times10^{15}$ cm$^{-3}$ at $T$ = 300 K for the cubical crystal FM lattice with the lattice constant $a$ = 0.23 nm. At the distance $r_0$ the exchange interaction $J_1$ has a maximum opposite value. If the accumulation layer (quantum well) contains a great number of electron states, the distance $r_0$ can be evaluated as the half of the period of the Ruderman-Kittel function, $r_0 \approx \frac{1}{2}(\pi/3n_s)^{1/3}$ [34, 35, 36], where $n_s$ is the electron density at the interface.

In order to find the spin-dependent potential barrier, we assume that the magnetic field $\vec{H}$ is parallel to the axis Oz. Then, the height of the energy barrier formed by the effective exchange interaction for injected spin-polarized electrons, which move from the interface, is determined by the relation

$$W = \sum_{\vec{R}} \int \langle\sigma_z^{(in)}(\vec{r})\rangle J^{(\mathrm{eff})}(\vec{r}, \vec{R}, 0) \langle S_z(\vec{R})\rangle_0 \, d\vec{r}, \tag{9}$$

where $\langle\sigma_z^{(in)}(\vec{r})\rangle = \langle\psi_\uparrow^{(in)*}(\vec{r})\psi_\uparrow^{(in)}(\vec{r}) - \psi_\downarrow^{(in)*}(\vec{r})\psi_\downarrow^{(in)}(\vec{r})\rangle$, $\langle S_z(\vec{R})\rangle_0$ is the $z$-projection of the statistical-average $d$-electron spin at the site $\vec{R}$ at the interface. For calculation of $W$ we assume that the spin density $\langle\sigma_z^{(in)}(\vec{r})\rangle = 1/2 \cdot \delta(r - r_0)$. We have found, that, if the accumulation layer contains a small number of localized electron states $\chi_\nu(x)$, which are determined by equation (2), then these states give the main contribution to the exchange interaction $J_1$ in equation (8) and to the height of the energy barrier $W$ (9). The maximum of the barrier is observed, when the accumulation layer has two sublevels of an exchange-splitted localized electron state (Figure 15). Exchange-splitted localized states

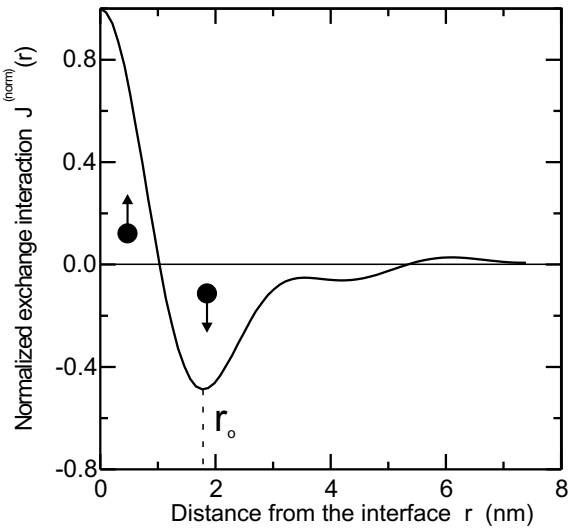


Figure 17. Normalized exchange interaction $J^{(\mathrm{norm})}(r) = J_1(\vec{r},0,0)/J_1(0,0,0)$ for the heterostructure with the difference of chemical potentials $\Delta\mu$ = 150 meV and with the electron concentration $n_0$ = $1\times10^{15}$ cm$^{-3}$ in the SC at $T$ = 300 K.

have high values of the exchange energy $\varepsilon_\lambda^{(\mathrm{ex})}$ (6) and this causes to high values of the barrier $W$ (9). If the accumulation layer does not contain localized states, the magnitude of $W$ sharply falls.

Figure 18 shows the energy barrier $W$ versus the difference of chemical potentials $\Delta\mu$ between the SC and the FM with the electron concentration $n_0$ = $1\cdot10^{15}$ cm$^{-3}$ in the SC at $T$ = 300 K. It can be seen that the height of the energy barrier has the maximum value at $\Delta\mu$ = 220 meV. The maximum of the barrier is due to the presence of localized electron states at the interface. We have found, that localized states $\chi_\nu(x)$, which are determined by equation (2), give the main contribution to the exchange interaction $J_1$ in equation (8). If the difference $\Delta\mu$ is small, the accumulation well is shallow and wide. This results in a low electron concentration at the interface and gives low values of the barrier height $W$. If the difference $\Delta\mu$ is greater than 220 meV, the accumulation well is thin. Despite the fact that the electron concentration at the interface is high, the number of localized electron states in thin well sharply decreases with

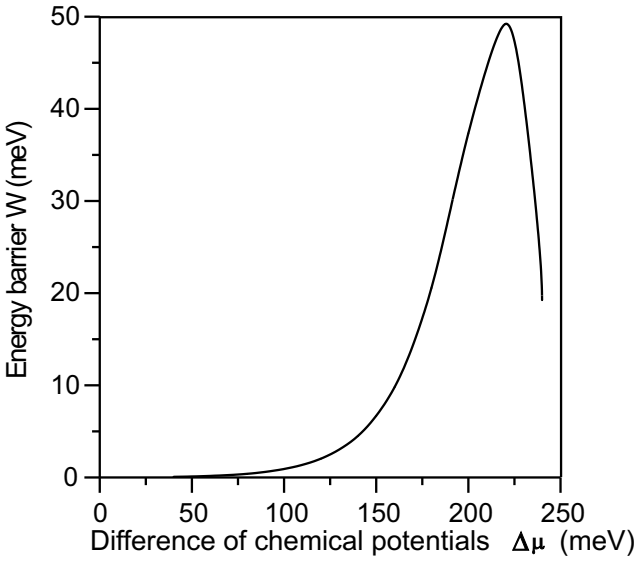


Figure 18. Potential barrier height $W$ versus the difference of chemical potentials $\Delta\mu$ in the heterostructure at $T$ = 300 K. The electron concentration $n_0$ in the SC is equal to $1{\cdot}10^{15}$ cm$^{-3}$.

decreasing thickness. If the accumulation well does not contain localized states, the magnitude of $W$ falls. The maximum of the barrier is observed, when the accumulation well has a small number of localized electron states. For the maximum height of the barrier, the electron concentration at the interface is equal to $0.66{\cdot}10^{19}$ cm$^{-3}$.

The temperature dependencies of the potential barrier $W$ are presented in figure 19 for heterostructures with the electron concentration $n_0 = 1{\cdot}10^{15}$ cm$^{-3}$ (at $T$ = 300 K) in the SC with various values of the difference of chemical potentials $\Delta\mu$. At the interface the electron concentration increases with temperature increasing. At low temperatures this causes the growth of the barrier $W$. At a certain temperature the magnitude of $W$ reaches the maximum value. The further temperature growth gives higher electron concentrations at the interface and results in the thin accumulation well with a small number of localized electron states. As a result of the decrease of the number of localized states and their further disappearance with decreasing thickness of the accumulation well,

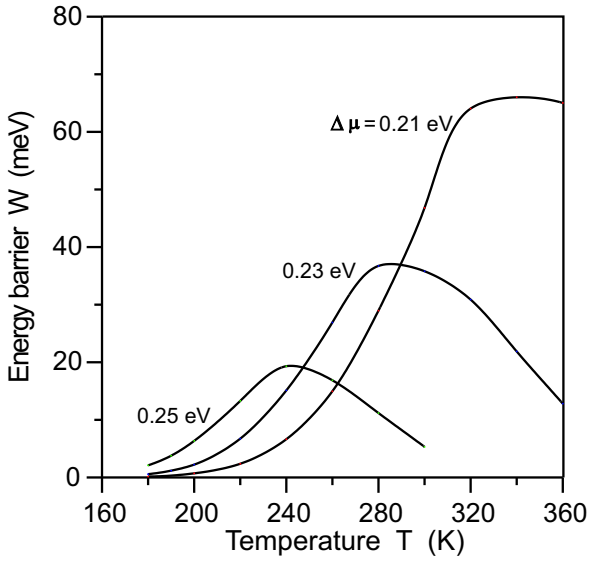


Figure 19. Temperature dependencies of the potential barrier height $W$ for heterostructures with the difference of chemical potentials $\Delta\mu$ = 0.21; 0.23; 0.25 eV. The electron concentration $n_0$ in the SC is equal to $1{\cdot}10^{15}$ cm$^{-3}$ at $T$ = 300 K.

the height of the potential barrier decreases.

### 3.4. The Backscattering Process of Injected Electrons on Exchange-Splitted Levels and Electron Accumulation in the Interface Quantum Well

The backscattering process of injected electrons on exchange-splitted levels of quantum well (QW) at the interface in heterostructures consisted of semiconductor / granular film with ferromagnetic metal nanoparticles is of great importance for the IMR effect. If one of the exchange-splitted levels lies in the top region of the QW and the energy of injected electrons is close to the energy of localized electron on this level, the backward scattering becomes dependent on spins of injected electrons. Accumulation of backscattered electrons in the QW leads to considerable reduction of the current depended on its spin orientation.

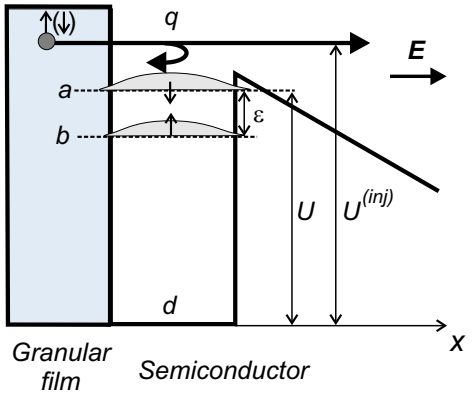


Figure 20. Backward scattering of injected electron on exchange-splitted levels in the quantum well in the granular film / semiconductor heterostructure. $E$ is the applied electric field, $U^{(inj)}$ and $U$ are the energies of injected electron and the top sublevel $a$, respectively.

The effect of spin-dependent current reduction can explain large values of the injection magnetoresistance in $SiO_2$(Co)/GaAs heterostructures. For simplicity we consider the current-reduction effect for the case of the square QW.

### 3.4.1. Spin-Dependent Electron Backscattering on the Quantum Well

Let us consider the backward scattering of injected electrons on exchange-splitted levels of the QW at the interface of a granular film / semiconductor heterostructure (Figure 20). Granular film contains ferromagnetic metal nanoparticles in an insulator matrix. Concentration of metal nanoparticles is sufficient to provide electrical conductivity of the granular film. Exchange interaction between electrons in the ferromagnetic metal and electrons in the QW splits electron levels in the QW. We assume that splitted electron levels (sublevels $a$ and $b$ in Figure 20) are filled by electrons. Electrons on exchange-splitted sublevels have opposite spin orientations. Difference of their energies is equal to the exchange energy $\varepsilon$. For clarification of the main features of scattering dependencies we restrict our consideration on the backscattering process on one of exchange-splitted levels – the top sublevel $a$ with a certain spin orientation. Electron backscattering on the sublevel $b$ is analogous.

The electron wavefunction on the sublevel $a$ is the product of the spatial function $u(x)$ and the spin function $\chi_u(\sigma_u)$

$$\psi(x, \sigma_u) = u(x)\chi_u(\sigma_u),$$

where $\sigma_u = \uparrow, \downarrow$ is the electron spin. In the WKB (Wentzel-Kramers-Brillouin) approximation [38] the spatial function in the QW can be written as

$$u(x) = \frac{C_u}{\sqrt{|k|}} \sin(kx + \pi/4), \tag{10}$$

where $k = \sqrt{2mU}/\hbar = \pi(n + 1/2)/d$ is the wavevector of the electron on the sublevel $a$ in the zero approximation with respect to $\varepsilon/U \ll 1$, $m$ is the electron mass, $U$ is the energy counted from the QW bottom, $d$ is the width of the QW, $C_u$ is the normalization coefficient, and $n = 0, 1, 2, \ldots$

The wavefunction of injected electron flying over the QW has the form of the product of the spatial function $v(x)$ and the spin function $\chi_v(\sigma_v)$

$$\varphi(x, \sigma_v) = v(x)\chi_v(\sigma_v),$$

where

$$v(x) = \frac{C_v}{\sqrt{|q|}} \exp(iqx), \tag{11}$$

$q = \sqrt{2mU^{(inj)}}/\hbar$, $U^{(inj)}$ is the energy counted from the QW bottom, $C_v$ is the normalization coefficient.

If the injected electron interacts with the electron localized on the sublevel $a$, then in the first approximation with respect to the interaction $W(x)$ the probability of the backscattering per unit time is [38]

$$P = \frac{2\pi}{\hbar} \left|\langle \Phi_f | W | \Phi_{in} \rangle\right|^2 \eta(U_f), \tag{12}$$

where $\eta(U_f)$ is the density of final states at the energy $U_f$, $\langle \Phi_f|$ is the final wavefunction, and $|\Phi_{in}\rangle$ is the initial wavefunction combined of injected and localized electrons.

If electrons form the singlet spin configuration ($\sigma_u = \uparrow$, $\sigma_v = \downarrow$ or $\sigma_u = \downarrow$, $\sigma_v = \uparrow$), then spatial parts of wavefunctions have the symmetric combination

$$\Phi_{in}(x_1, x_2) = u(x_1)v(x_2) + u(x_2)v(x_1),$$

$$\Phi_f(x_1, x_2) = u(x_1)\bar{v}(x_2) + u(x_2)\bar{v}(x_1),$$

where $\bar{v}(x)$ is the wavefunction of the backscattered electron described by Eq. (11) with the substitution $q \to -q$. For the singlet spin state the backscattering probability (12) is equal to

$$P_S = \frac{8\pi\eta(U_f)}{\hbar} |A + B|^2 , \tag{13}$$

where

$$A = \int_0^d u^*(x_1)\bar{v}^*(x_2)W(x_1 - x_2)u(x_1)v(x_2)\, dx_1 dx_2,$$

$$B = \int_0^d u^*(x_2)\bar{v}^*(x_1)W(x_1 - x_2)u(x_1)v(x_2)\, dx_1 dx_2,$$

If electrons form the triplet spin configuration ($\sigma_u =\uparrow$, $\sigma_v =\uparrow$ or $\sigma_u =\downarrow$, $\sigma_v =\downarrow$), then spatial parts of wavefunctions are antisymmetric

$$\Phi_{in}(x_1, x_2) = u(x_1)v(x_2) - u(x_2)v(x_1),$$

$$\Phi_f(x_1, x_2) = u(x_1)\bar{v}(x_2) - u(x_2)\bar{v}(x_1).$$

For the triplet state the probability (12) can be written as

$$P_T = \frac{8\pi\eta(U_f)}{\hbar} |A - B|^2 . \tag{14}$$

Magnitudes $A$ and $B$ in relations (13) and (14) are functions of wavevectors $q$ and $k$. Besides, the wavevector $k$ depends on the number $n$ of localized level: $kd = \pi(n + 1/2)$. Taking into account wavefunction forms (10) and (11), for the uniform interaction $W(x) = W$ we obtain

$$A = \frac{C_u^2 C_v^2 W(kd + 1)}{4ik^2q^2} [\exp(2iqd) - 1]$$

$$B = \frac{C_u^2 C_v^2 W}{2kq(k^2 - q^2)^2} [(-1)^n \exp(iqd)(iq + k)$$

$$-(iq - k)]^2 .$$

Probabilities $P_S$ (13) and $P_T$ (14) strongly depend on the wavevector

$$q = \frac{\sqrt{2mU^{(inj)}}}{\hbar} = \left[\frac{\pi^2(n + 1/2)^2}{d^2} + \frac{2m\Delta U}{\hbar^2}\right]^{1/2}$$

and, consequently, on the difference $\Delta U$ between the energy of injected electron $U^{(inj)} = U + \Delta U$ and the energy of localized electron $U$ in the QW. Singlet and triplet backscattering probabilities versus the difference $\Delta U$ for $n = 0$ are shown in Figure 21. The difference $\Delta U$ is normalized by the QW width $d$ and the probabilities are normalized by the magnitude of the singlet probability $P_S^{(0)}$ at $\Delta U = 0$. It is necessary to notice that for small values of $\Delta U$ ($< V_0/d^2$) the probability of the singlet backscattering $P_S$ is higher than the triplet backscattering probability $P_T$ and, therefore, the backward scattering becomes strongly dependent on spins of injected electrons. For $\Delta U \to 0$ the ratio of singlet and triplet probabilities of backscattering leads to the relation

$$\frac{P_S}{P_T} \to \left(\frac{\pi + 6}{\pi - 2}\right)^2 = 64.1.$$

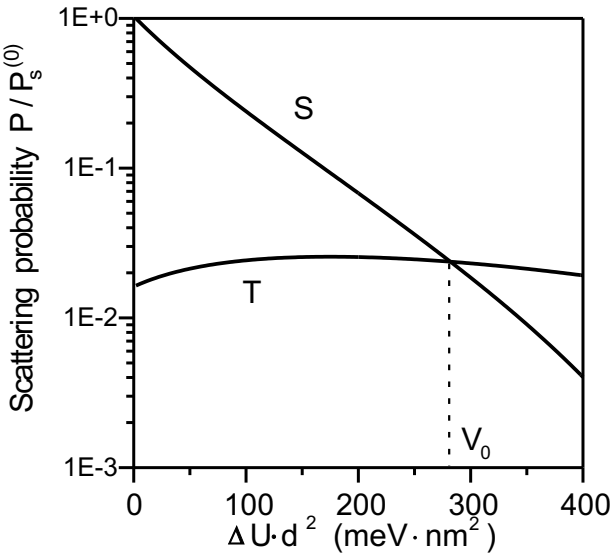


Figure 21. Probabilities of singlet (S) and triplet (T) backscattering of injected electron on the top sublevel $a$ (Figure 20) of the QW versus the parameter $\Delta U d^2$, where $\Delta U$ is the difference between the energy of electron and the energy of the sublevel $a$, and $d$ is the QW width. Probabilities are normalized by the magnitude of the singlet probability $P_S^{(0)}$ at $\Delta U = 0$.

The backscattering probability reduces with growth of $\Delta U$. Thus, the backscattering process becomes important, if (1) one sublevel of the exchange-splitted level with a certain spin orientation lies at the top of the QW and (2) the energy of injected electrons is close to the energy of localized electron on this sublevel.

### 3.4.2. Spin-Dependent Current Reduction

Let us consider the current reduction induced by the backward scattering of injected electrons on the QW with exchange-splitted levels at the interface of a granular film / semiconductor heterostructure. We assume that the difference between the energy of injected electrons and the energy of the top sublevel is less than the exchange energy, $\Delta U < \varepsilon$ (Figure 20). Therefore, we restrict our consideration on singlet and triplet electron backscattering processes on the top sublevel $a$ of the top exchange-splitted level (Figure 22). We assume that the sublevel $b$ lies below the sublevel $a$. The capture of backscattered electrons by the QW leads to the considerable current reduction depended on spin orientation of injected electrons. If the Fermi level lies below the localized top electron level in the QW, then at a finite temperature sublevels of this exchange-splitted level are partially filled by electrons. Backscattered electrons can be captured by the QW and, in accordance with their spin orientation, they occupy different localized sublevels. We suppose that the spin relaxation time is greater than the storage time of additional electrons in the QW. Then, for the singlet scattering process backscattered electrons occupy the sublevel $b$ with the spin orientation opposite to the spin orientation of the sublevel $a$ (Figure 22a). On the contrary, for the triplet case backscattered electrons fall on the sublevel $a$ (Figure 22b). The storage time $\tau$ of the presence of additional electrons in the QW depends on the electron-hole recombination, on temperature activation processes, and on the electron tunneling into the conduction band. For underlying levels the storage time $\tau$ is greater than the storage time of electrons on overlying ones. The additional charge in the QW leads to the electrostatic blockade of injected electrons and to a current reduction. In this way, the current flowing in the heterostructure with QW, which contains exchange-splitted levels, is unstable. Due to the backscattering process and accumulation of electrons in the QW, small values of the interaction $W(x)$ between injected electrons and electrons localized on the level $a$ in relation (12) leads to the additional Coulomb repulsion for injected electrons and to high values of the current reduction.

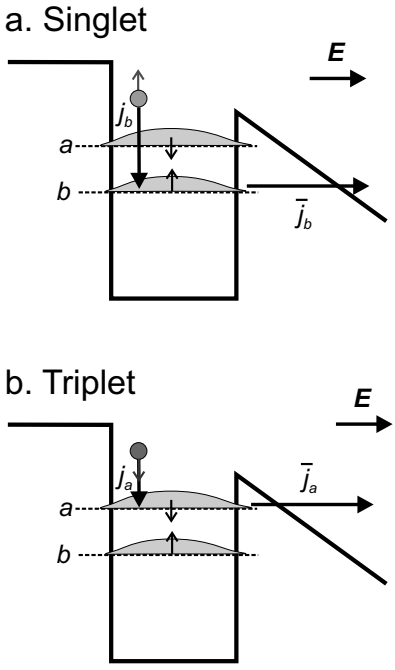


Figure 22. Accumulation of backscattered electrons in the QW with exchange-splitted levels in the singlet (a) and in the triplet (b) backscattering processes.

Let us calculate the reduction of the current. The current density flowing over the QW is equal to

$$j = en\mu E, \tag{15}$$

where $e$ is the electron charge, $\mu$ is the electron mobility, $E$ is the electric field,

$$n = n_0 \exp\left(\frac{-e\varphi}{kT}\right) \tag{16}$$

is the electron concentration over the QW, $n_0$ is the electron concentration without an electric field, $\varphi$ is the potential of the field of additional localized electrons in the QW, $k$ is the Boltzmann constant, and $T$ is the temperature.

In the singlet backscattering case, the additional charge accumulates on the sublevel $b$ (Figure 22a). The potential $\varphi$ of the field caused by this additional

charge is determined by the equation [39]

$$\frac{d^2\varphi}{dx^2} = \frac{4\pi e}{\bar{\varepsilon}}(n_b - n_b^{(0)}), \tag{17}$$

where $\bar{\varepsilon}$ is the dielectric permittivity of the semiconductor in the QW region; $n_b$ and $n_b^{(0)}$ are electron concentrations on the sublevel $b$ in the electric field and without a field, respectively. If the additional concentration of the charge $n_b - n_b^{(0)}$ is uniformly distributed over the QW width, then the solution of Eq. (17) is given by

$$\varphi(x) = \frac{2\pi e}{\bar{\varepsilon}}(n_b - n_b^{(0)})x^2.$$

Injected electrons must surmount the additional barrier with the energy height

$$e\varphi = \frac{2\pi e^2}{\bar{\varepsilon}}(n_b - n_b^{(0)})d^2. \tag{18}$$

Taking into account relations (13), (15), (16), and (18), we obtain the current density of electrons incoming on the sublevel $b$

$$j_b = P_S j = P_S e\mu E n_0 \exp\left[\frac{-2\pi e^2(n_b - n_b^{(0)})d^2}{\bar{\varepsilon}kT}\right].$$

Release of additional electrons from the sublevel $b$ is determined by the time $\tau_b$ and the current density of outgoing electrons can be written as

$$\bar{j}_b = \frac{e(n_b - n_b^{(0)})d}{\tau_b}.$$

For the equilibrium process $j_b = \bar{j}_b$ and

$$P_S\mu E n_0 \exp\left[\frac{-2\pi e^2(n_b - n_b^{(0)})d^2}{\bar{\varepsilon}kT}\right] = \frac{(n_b - n_b^{(0)})d}{\tau_b}. \tag{19}$$

Relation (19) is the equation in the unknown additional electron concentration $n_b - n_b^{(0)}$. Taking into account relations (15), (16) and solution of equation (19), we find the current reduction caused by the singlet electron backscattering on the QW as the ratio of the current $j$ flowing in the heterostructure without

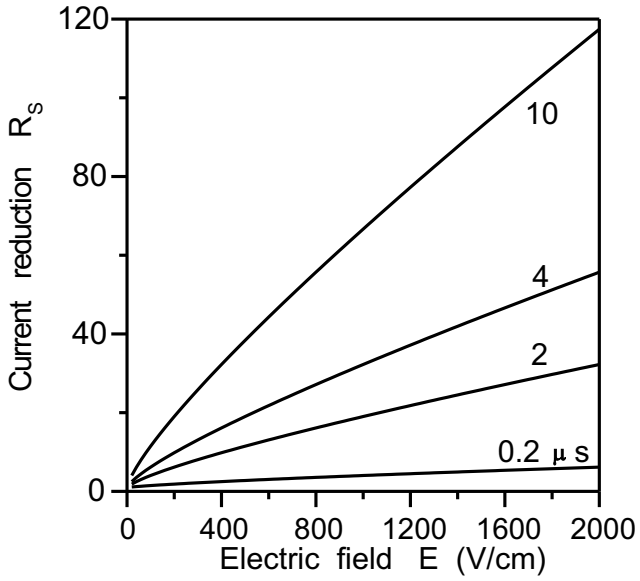


Figure 23. Current reduction $R_S$ versus the applied electric field $E$ for different storage time $\tau_b$ of electrons in the QW. The backscattering probability $P_S = 2 \cdot 10^{-6}$, the width of the QW $d = 2$ nm, temperature $T = 300$ K, and the electron concentration in the semiconductor $n_0 = 2.5 \cdot 10^{17}$ cm$^{-3}$.

additional charge in the QW and the current $j_\varphi^{(S)}$ flowing in the heterostructure with the charge in the QW, respectively,

$$R_S = \frac{j}{j_\varphi^{(S)}} = \exp\left[\frac{2\pi e^2 (n_b - n_b^{(0)}) d^2}{\bar{\varepsilon} k T}\right]. \tag{20}$$

The current reduction $R_S$ versus the applied electric field $E$ for different times $\tau_b$ is shown in Figure 23. Calculations are performed for $P_S = 2 \cdot 10^{-6}$, width of the QW $d = 2$ nm, permittivity $\bar{\varepsilon} = 1$, $T = 300$ K, $\mu = 8 \cdot 10^3$ cm$^2$/V·s, and $n_0 = 2.5 \cdot 10^{17}$ cm$^{-3}$. From the presented dependencies we can see that backscattering of injected electrons on exchange-splitted levels and accumulation of electrons in the QW leads to considerable reduction of the current.

If the difference $\Delta U = U^{(inj)} - U$ between the energy of electron and the energy of the sublevel $a$ is low, the probability of the backscattering pro-

cess $P_S$ and the current reduction $R_S$ are of high values. Figure 24 presents current reduction $R_S$ versus the difference $\Delta U$ for different storage time $\tau_b$ of electrons in the QW. One can see that the current-reduction effect caused by the backscattering is sharply decreased and $R_S \to 1$ with increase of the difference $\Delta U$.

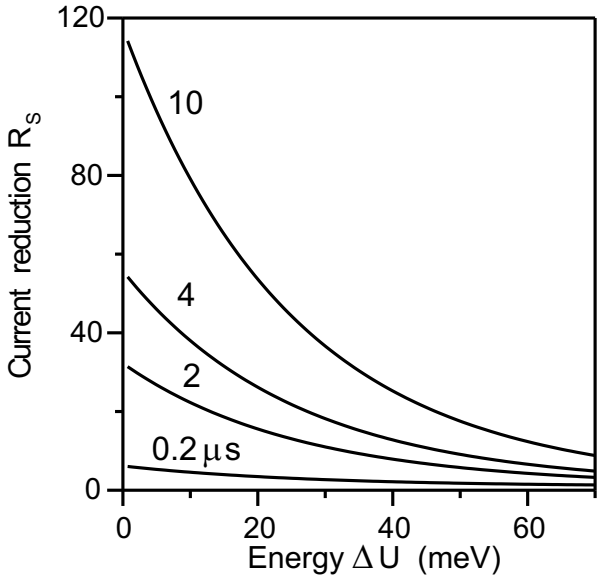


Figure 24. Current reduction $R_S$ caused by the singlet electron backscattering in granular film / semiconductor heterostructure with QW contained exchange-splitted levels versus the difference $\Delta U$ between the energy of electron and the energy of the top level for different storage time $\tau_b$ of electrons in the QW. The backscattering probability $P_S = 2 \cdot 10^{-6}$, the applied electric field $E = 2000$ V/cm, the width of the QW $d = 2$ nm, temperature $T = 300$ K, and the electron concentration in the semiconductor $n_0 = 2.5 \cdot 10^{17}$ cm$^{-3}$.

The current reduction depends on the electron concentration $n_0$ in the semiconductor. For small values of $n_0$ the additional concentration $n_b - n_b^{(0)}$ in Eq. (19) leads to zero and the reduction is small, $R_S \to 1$. For great values of the concentration $n_0$ (for example, close to metal concentrations) the QW contains filled levels and the additional charge in the QW is impossible. As a result of

this, there is no any reduction of the current.

In the triplet backscattering case, the additional charge accumulates on the sublevel $a$ (Figure 22b). By analogy with the singlet backscattering (19), the additional charge concentration $n_a - n_a^{(0)}$ on the sublevel $a$ is determined by equation

$$P_T \mu E n_0 \exp\left[\frac{-2\pi e^2 (n_a - n_a^{(0)}) d^2}{\bar{\varepsilon} kT}\right] = \frac{(n_a - n_a^{(0)}) d}{\tau_a},$$

where $\tau_a$ is the storage time of the additional charge on the sublevel $a$, $P_T$ is the triplet backscattering probability. The current reduction is

$$R_T = \frac{j}{j_\varphi^{(T)}} = \exp\left[\frac{2\pi e^2 (n_a - n_a^{(0)}) d^2}{\bar{\varepsilon} kT}\right]. \tag{21}$$

where $j_\varphi^{(T)}$ is the current flowing in the heterostructure with the charge in the QW. In comparison with the singlet case, for $\tau_a \ll \tau_b$ and $P_T < P_S$ the current reduction $R_T$ caused by the triplet backscattering and by the accumulation of injected electrons in the QW is insignificant. Thus, the backscattering of injected electrons on exchange-splitted levels and accumulation of electrons in the QW leads to the current reduction depended on spins.

The effect of spin-dependent current reduction can explain large values of the giant injection magnetoresistance in $SiO_2$(Co)/GaAs heterostructures. The $2D$ QW (accumulation electron layer) with exchange-splitted levels is formed at the interface in the GaAs (Figure 15). Electrons localized in the QW form the potential barrier for injected electrons. The applied magnetic field increases the height and reduces the transparency of the barrier. This leads to increase of the backscattering probability $P_S$ and the current reduction $R_S$. Thus, accumulation of additional charge in QW leads to the spin-dependent current reduction and results in significant amplification of the magnetoresistance effect. In the non-avalanche regime the current reduction reaches the value of 52 at room temperature (Figure 6a).

### 3.5. Positive Feedback Caused by the Avalanche Process

At high voltages, the layer with strong electrical field with the thickness $d$ is formed in the SC and the potential drops rapidly in the strong-field layer close to the barrier (Figure 25) [7]. The avalanche process is induced by electrons

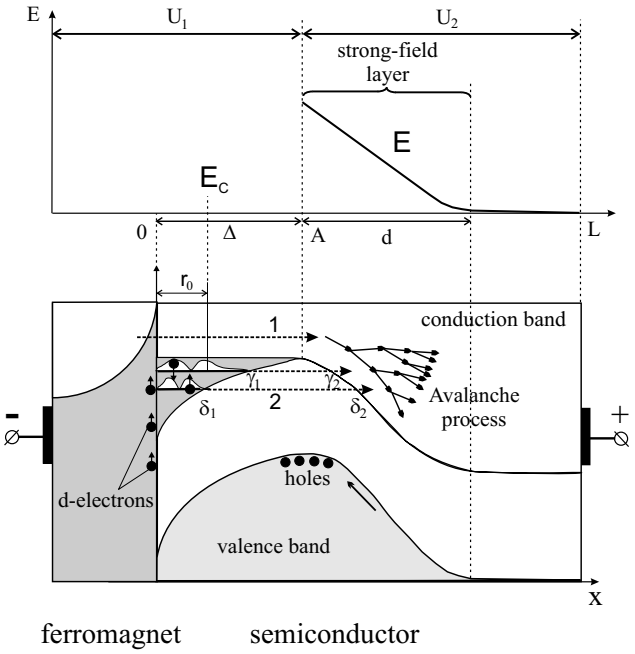


Figure 25. Schematic band diagram at the applied electrical field in the ferromagnet / semiconductor and electrical field distribution in the semiconductor at a high voltage in the avalanche regime. The avalanche process is induced by electrons, which (1) surmount over the spin-dependent potential barrier formed by localized states at the distance $r_0$ from the interface, (2) tunnel from exchange-splitted localized states.

and originates in the vicinity region of the barrier. Holes are arisen during the impact ionization, move to the maximum of the valence band (point $A$), are accumulated in the region of the point $A$ and disappear by recombination in this region. Existence of holes in the region of the barrier lowers the barrier height, grows the electron current flowing through the barrier and leads to the enhancement of the avalanche process. Due to the formed positive feedback small variations in the barrier height give great changes in the current.

### 3.6. The IMR Effect

The observed IMR effect can be explained by the developed theoretical model. Action of the applied magnetic field results in two effects: (1) the domain structure of the granular film changes, (2) spins of ferromagnetic particles and localized electrons at the interface are aligned along the field direction. This leads to the growth of the barrier height, reduces the barrier transparency and decreases the electron concentration at the barrier region. Due to spin-dependent electron backscattering on the quantum well and the feedback formed in the avalanche process, small variations in the barrier height and its transparency lead to great changes in the current.

Two ways of the spin-polarized current injected into the SC can be supposed (Figure 25): (1) injected electrons surmount the spin-dependent potential barrier $W$ at the distance $r_0$ from the interface, (2) spin-polarized electrons tunnel from sublevels of the exchange-splitted localized states. If the magnetic field $H$ is less than the saturation field $H_{sat}$, in which domains disappear, the domain structure of the granular film (Figure 1) induces corresponding spin orientations of electrons localized in the accumulation layer in the SC and this induced domain structure has domain walls (Figure 26). In this case, electrons injected from the granular film can cross through the accumulation layer without a loss of their spin polarization and without surmounting the potential barrier on channels close to domain walls (trajectories with points $a$). The average concentration of electrons, which trigger the avalanche process, is given by the sum of electron concentrations in regions with maximum height of the spin-dependent potential barrier (surface $C$ in Figure 26)

$$n_C = n_a \xi_a + n_b \xi_b, \tag{22}$$

where $n_a$ is the electron concentration in regions of domain walls, $n_b$ is the electron concentration in domain regions, $\xi_a$ and $\xi_b$ are contributions of partial concentrations to the average concentration. In the saturation magnetic field, $H = H_{sat}$, when domains disappear, electrons moving in the SC from the interface must surmount the potential barrier at the distance $r_0$ (trajectories with points $b$) and $\xi_a = 0$ in equation (22). Taking into account that $n_a > n_b$ and the growth of the magnetic field reduces the contribution $\xi_a$ of domain walls, from equation (22) one can find that in the range $[0, H_{sat}]$ increasing magnetic field leads to reduction of the electron concentration $n_C$.

At last, consider the barrier at the magnetic field $H > H_{sat}$. The applied magnetic field $H$ presented in the Hamiltonian $\mathcal{H}_s$ interacts with spins $\vec{\sigma}(\vec{r})$ and

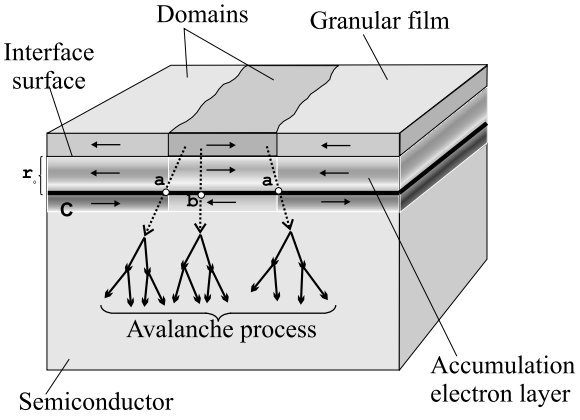


Figure 26. Trajectories without spin-flip scattering of injected electrons and without surmounting the potential barrier on the accumulation layer (points $a$) and trajectories with surmounting the potential barrier (points $b$). Surface $C$ is the surface of maximum heights of the spin-dependent potential barrier.

$\vec{S}(\vec{r})$. For the magnetic field $H > H_{sat}$ there is alignment of spins of electrons in the accumulation layer and spins of ferromagnetic particles in the granular film with increasing magnetic field. Magnetic field polarizes spins along the field direction. The field growth leads to the increase of the $z$-projection $\langle S_z(\vec{R})\rangle_0$, to the growth of the barrier height $W$ (9) and to the reduction of the concentration $n_b$ in equation (22). In this case, in the absence of domain walls, $\xi_a = 0$ and $\xi_b = 1$.

The avalanche process originates in the vicinity region of the barrier. The current density $j$ flowing in the heterostructure is determined by the concentration of injected electrons $n_C$ (equation (22)), the electron mobility $\mu_e$ and the electrical field $E_C$ at the surface $C$, $j = en_C\mu_e E_C$. Then, taking into account that $n_a = n_{int}\exp(eU_C/kT)$, $n_b = n_{int}\exp[(eU_C - W)/kT]$, where $n_{int}$ is the electron concentration at the interface at the Fermi level, $U_C$ is the difference of potentials between the interface and the surface $C$, from equation (1) we get

$$IMR[W(H), T] = \frac{n_C(0)E_C(0)}{n_C(H)E_C(H)} - 1$$

$$= \frac{\{\xi_a(0) + \xi_b(0)\exp[-W(0)/kT]\}E_C(0)}{\{\xi_a(H) + \xi_b(H)\exp[-W(H)/kT]\}E_C(H)} - 1. \quad (23)$$

If $W(0) \gg kT$, for $H > H_{sat}$ contribution coefficients $\xi_a(H) = 0$, $\xi_b(H) = 1$ and the magnetoresistance *IMR* (23) is rewritten in the simple form

$$\textit{IMR}[W(H), T] = A\exp\left[\frac{W(H)}{kT}\right] - 1, \quad (24)$$

where $A = \xi_a(0)E_C(0)/E_C(H)$. Taking into account that the energy barrier $W(H)$ sharply depends on temperature [5], in the first approximation the temperature dependence of the *IMR* is determined by the term $\exp[W(H)/kT]$. The dependence of the *IMR* on the applied electrical field is determined by the coefficient $A$. It depends on the ratio of the electrical field $E_C$ at the surface $C$ in the absence of a magnetic field and in the magnetic field $H$, respectively. When the avalanche process has been developed in the absence of a magnetic field, the electrical field $E_C(0)$ is high. When the magnetic field suppresses the onset of the impact ionization, distribution of the applied voltage $U = U_1 + U_2$ (Figure 25) changes. In the absence of the avalanche process the voltage $U_2$ is equal to a high value. This causes decreasing the voltage $U_1$ and decreasing the field $E_C(H)$ with respect to the field $E_C(0)$ without a magnetic field. The coefficient $A$ leads to high values.

## 4. Explanation of the Experiment

In order to explain high values of the IMR effect in $SiO_2$(Co)/GaAs heterostructures and the temperature-peak type character, we use the developed theoretical model. The developed theory can be applied for these heterostructures, if the size of Co nanoparticles is less than the thickness $l$ of the accumulation layer. In this case, the granular film can be considered as continuous and can be characterized by statistical-average parameters. The thickness $l$ depends on the difference of the chemical potentials $\Delta\mu = \mu_g - \mu_s$, where $\mu_s$ is the chemical potential in the SC and $\mu_g$ is the chemical potential in the granular film. In the first approximation, the chemical potential $\mu_g$ is given by

$$\mu_g = \mu_{\mathrm{SiO_2}}(x_{\mathrm{SiO_2}}/100) + \mu_{\mathrm{Co}}(x_{\mathrm{Co}}/100),$$

where $\mu_{SiO_2}$, $\mu_{Co}$ are the chemical potentials of the $SiO_2$ matrix and Co nanoparticles; $x_{SiO_2}$, $x_{Co}$ are the atomic concentrations of the $SiO_2$ and Co in percents, respectively. The difference $\Delta\mu$ between chemical potentials of the GaAs and the $SiO_2$(Co) granular film and between chemical potentials of the Si substrate and the granular film can be estimated from well known values of the energy of the thermoelectron emission. For the given materials the differences of the chemical potentials are $\mu_{SiO_2} - \mu_{Co}$ = 0.59 eV, $\mu_{SiO_2} - \mu_{GaAs}$ = 0.62 eV, $\mu_{Co} - \mu_{GaAs}$ = 0.03 eV, $\mu_{SiO_2} - \mu_{Si}$ = 0.95 eV, $\mu_{Co} - \mu_{Si}$ = 0.36 eV [40].

In order to solve equations (2), (3), (7) in the approximation of the continuous granular film model, we need to find the surface probability of the Co particle distribution at the interface. We assume that at the interface Co particles are randomly allocated with the surface probability

$$s = \bar{p}^{2/3} = \left[\frac{x_{Co} v_{Co}}{x_{Co} v_{Co} + (100 - x_{Co}) v_{SiO_2}}\right]^{2/3},$$

where $\bar{p}$ is the relative Co volume, $v_{Co} = m_{Co}/\varrho_{Co} N_A$, $v_{SiO_2} = m_{SiO_2}/\varrho_{SiO_2} N_A$ are atomic and molecular volumes for the Co and the $SiO_2$ matrix; $m_{Co}$, $m_{SiO_2}$ are the respective atomic and molecular masses; $\varrho_{Co}$, $\varrho_{SiO_2}$ are the densities of Co particles and the $SiO_2$ matrix; $N_A$ is the Avogadro number. For calculations we use $m_{Co}$ = 58.93 a.m., $m_{SiO_2}$ = 60.09 a.m., $\varrho_{Co}$ = 8.90 g/cm$^3$, $\varrho_{SiO_2}$ = 2.26 g/cm$^3$ [41]. According to the continuous granular film approximation, we must made substitutions $\langle \vec{S}(\vec{R}) \rangle_0 \rightarrow s \langle \vec{S}(\vec{R}) \rangle_0$ and $\langle S_z(\vec{R}) \rangle_0 \rightarrow s \langle S_z(\vec{R}) \rangle_0$ in relations (6) and (9), respectively.

Using the developed model, we have found the electron wavefunction $\chi_\nu(x)$ (2), the inner self-consistent electrical field $\varphi(\vec{r})$ (3), and the energy barrier $W$ (9). Calculations have been made for the effective exchange interaction $J_0(\vec{r} - \vec{R}) = J_0 \exp(-\xi|\vec{r} - \vec{R}|)$ with $J_0$ = 2 eV, $\xi$ = 2 nm$^{-1}$ [37]. For $SiO_2$(Co)/GaAs heterostructures at the given temperatures 160 - 340°C the thickness $l$ of the accumulation layer is in the range 8 - 50 nm. The size of Co nanoparticles is less than the thickness $l$, and the approximation of the continuous granular film is truthful. Heterostructures possess localized electron states in the accumulation layer at the interface. In contrast, for $SiO_2$(Co)/Si heterostructures due to higher values of the difference of the chemical potentials $\Delta\mu$ at the interface the potential depth of the accumulation layer is deeper. This leads to higher electron concentration at the interface and to more efficient shielding of Co spins. As a result of this, the accumulation layer has small thickness without any localized states. The absence of localized states in $SiO_2$(Co)/Si

heterostructures explains small values of the barrier $W$ (9). Small height of the barrier results in small variations of $W$, when the magnetic field is changed, and small values of the IMR effect (Figures 11, 12) in comparison with *IMR* values in $SiO_2$(Co)/GaAs heterostructures (Figures 8, 9, 10, 13, 14). Let us consider *IMR* dependencies on the Co concentration, temperature and the magnetic field.

### 4.1. IMR Dependence on the Co Concentration

The dependence of the *IMR* on the Co concentration $x$ for $SiO_2$(Co)/GaAs structures, when electrons are injected from the $SiO_2$(Co) film (Figure 10), demonstrates high *IMR* values for the concentration range $x$ = 54 - 71 at.% and low *IMR* values for lower and higher Co concentrations. From the developed model it is found that structures with $x$ = 54 - 71 at.% have one - two electron localized states with high energies $\varepsilon_\lambda^{(\mathrm{ex})}$ (6), which leads to high barrier $W$ at room temperature. Heterostructures with lower Co concentration ($x < 54$ at.%) possess greater number of localized states in the accumulation layer with energies $\varepsilon_\lambda^{(\mathrm{ex})}$ of small values. For these structures the barrier height is small and the *IMR* coefficient is low. If the Co concentration $x > 71$ at.%, the accumulation layer has small thickness without localized states and is transparent for current. This leads to small *IMR* values, too.

### 4.2. Temperature Dependencies of the IMR

At the interface the electron concentration increases with temperature increasing. At low temperatures the accumulation layer contains large number of exchange-splitted localized states with small energies $\varepsilon_\lambda^{(\mathrm{ex})}$. Temperature increasing induces thinning of the accumulation layer, a decrease of the localized state number, an increase of energies $\varepsilon_\lambda^{(\mathrm{ex})}$, and a growth of the barrier $W$. At a certain temperature the accumulation layer contains one exchange-splitted level and the magnitude of $W$ reaches the maximum value. The further temperature growth gives higher electron concentration at the interface, more efficient shielding of Co spins, and thinner thickness of the accumulation layer. When the sublevel, on which electrons have spin orientations opposite to Co spins, crosses the Fermi level, the height of the potential barrier $W$ sharply decreases. In Figure 4 for the $SiO_2$(Co)/GaAs structure with the Co content 71 at.% crossing of the Fermi level is manifested as a fall on the temperature dependence of the inject current at $T$ = 320 K at the applied voltage $U$ = 70 V. This fall in the

current corresponds to the disappearance of the IMR effect at 320 K, $U$ = 70 V in Figure 13.

The temperature-peak type character of the IMR effect is presented in Figures 13, 14. Maxima of peaks correspond to one exchange-splitted level in the accumulation layer. Neglecting spin-polarized tunneling from exchange-splitted localized states, we fit experimental results using the relation (24). The barrier $W$ is given by equation (9) and the amplitude $A$ in the relation (24) is determined to reach the best fit of the peak height. According to the developed model, the peak width is inversely proportional to the magnitude of the surface probability $s$ of the Co particle distribution at the interface. Decreasing the Co content results in the decrease of the surface probability $s$: from $s$ = 0.52 ($x$ = 71 at.% Co) to $s$ = 0.26 ($x$ = 38 at.% Co). This corresponds to the observed increase of the peak width with Co concentration decreasing: from $\Delta T$ = 37 K ($x$ = 71 at.% Co) to $\Delta T$ = 62 K ($x$ = 38 at.% Co).

Locations of IMR temperature peaks can be shifted by the applied electrical field. These shifts can be explained by the change of the electron concentration at the interface under the electrical field action. The applied field causes to an electron depletion in the SC at the interface. As a result of this, at high field magnitudes it is need higher temperatures to form the accumulation layer with one exchange-splitted level. In order to take into account the action of the electrical field for the $SiO_2$(Co)/GaAs structure with the Co content 71 at.% in Figure 13, we use the following differences of the chemical potentials $\Delta\mu$: 0.201 eV ($U$ = 40 V), 0.197 eV ($U$ = 50 V), 0.187 eV ($U$ = 60 V and 70 V).

### 4.3. IMR Dependencies on the Magnetic Field

At last, we consider *IMR* dependencies on the magnetic field for $SiO_2$(Co)/GaAs structures. As we can see from Figure 9, at magnetic fields of low values the *IMR* grows greater than at high magnetic fields. The high growth of the *IMR* can be explained by changes of the domain structure, which disappears at $H_{sat}$ = 4 kOe. Slow *IMR* increasing at the magnetic field $H > H_{sat}$ can be due to alignment of different spin orientations of randomly allocated Co particles at the interface. Magnetic field polarizes spins along the field direction. This leads to the increase of the $z$-projection $\langle S_z(\vec{R})\rangle_0$ and to the increase of the barrier height $W$ (9) with growth of the magnetic field. Higher barrier height suppresses the onset of the avalanche process. This changes the potential distribution and decreases the electrical field $E_C(H)$ (Figures 25, 26) in comparison

with the electrical field $E_C(0)$ in the absence of a magnetic field. As a result of this the value of the coefficient $A$ in equation (24) becomes higher with magnetic field increasing.

# 5. Magnetic Sensors

## 5.1. Magnetic Sensors Based on $SiO_2$(Co)/GaAs Structures

High values of the *IMR* coefficient in $SiO_2$(Co)/GaAs structures give possibility to use these structures as sensitive magnetic sensors for low-field magnetic measurements. In this connection, in this section we present the *IMR* effect in magnetic fields of low values.

Dependencies of the *IMR* coefficient versus the applied magnetic field $H$ of low values for $SiO_2$(Co)/GaAs structure with 71 at. % Co (sample #4) are shown in Figure 27. The magnetic field is parallel to the film surface. Measurements were carried out at room temperature. Dependencies are of the linear type.

Dependencies of the *IMR* coefficient versus the applied voltages reveal a fine structure. This fine structure is not observed in high magnetic fields. Figure 28 presents the *IMR* value as a function of the applied voltage $U$ for $SiO_2$(Co)/GaAs structure with 71 at. % Co (sample #4) and for $SiO_2$(Co)/GaAs structure with 54 at. % Co (sample #3) in the magnetic field $H$ = 6.25 Oe. The onset of the avalanche process is observed at 66 - 67 V.

The peak-type character of the dependencies is explained by localized levels in the accumulation electron layer (2D quantum well, QW) in the GaAs near the interface (Figure 15) [5, 7]. Energies of the levels are determined by the QW width. Besides this, localized levels are splitted by the exchange interaction between electrons in the QW and $d$-electrons of Co nanoparticles. Electrons tunnel through the barrier from these levels and trigger the avalanche process. At voltages corresponded to the onset of the avalanche process electrons tunnel from the highest level. This electron tunneling corresponds to the first peak in Figure 28.

Growth of the applied voltage leads to a decrease of electrons on the highest level. The electron reduction on the highest level results in a decrease of the spin-dependent potential barrier. The further voltage growth changes the form of the QW and the slope of the conduction band in the vicinity of the QW (Figure 25). At a certain voltage, the possibility of electron tunneling from the level arranged lower the highest level becomes maximal. The electron tunneling

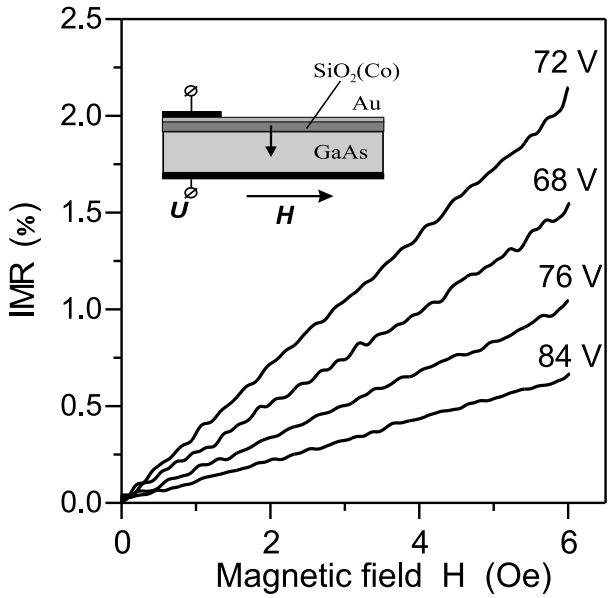


Figure 27. Dependencies of the *IMR* coefficient versus the applied magnetic field $H$ for $SiO_2$(Co)/GaAs structure with 71 at. % Co at different applied voltages.

from this level corresponds to the second peak. The further growth of the voltage leads to a devastation of this level. Electrons begin to tunnel from the third level and so on. One can say that each peak on the dependence of the *IMR* coefficient versus the applied voltage corresponds to the level in the QW in the case, when this level is filled by electrons, the possibility of electron tunneling is maximal and higher levels are not filled by electrons. Due to the hole positive feedback small variations in the tunneling and in the electron concentration on levels leads to significant variations of the current and increases the peak-type character of the dependence. We can see that dependencies of the *IMR* coefficient versus the applied voltages for $SiO_2$(Co)/GaAs heterostructures (Figure 28) are of the peak-type character with a complicated fine substructure. It can be supposed that the fine substructure is caused by variations in the width and in the depth of the QW over the interface surface. At low magnetic fields in the avalanche onset region the magnetoresistance reaches highest values. Thus, in order to obtain

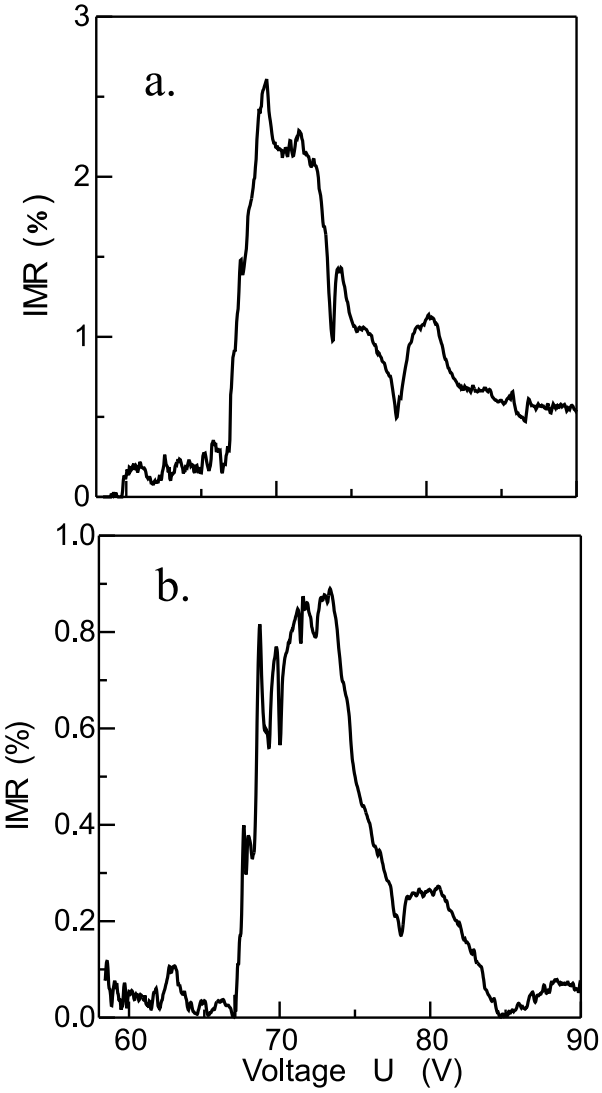


Figure 28. Dependencies of the *IMR* coefficient versus the applied voltages for $SiO_2$(Co)/GaAs structure with 71 at. % Co and for $SiO_2$(Co)/GaAs structure with 54 at. % Co in the magnetic field $H$ = 6.25 Oe.

high sensitivity of magnetic sensors based on $SiO_2$(Co)/GaAs heterostructures, it is necessary to apply voltages corresponded to the avalanche onset.

## 5.2. Extension of the IMR Effect on Heterostructures with Other Semiconductors

We have considered $SiO_2$(Co)/GaAs heterostructures and have come to the conclusion that these heterostructures can be used as (1) spin-polarized electron injectors and (2) efficient magnetoresistive sensors. Spin-polarized electron injection can be observed at low voltages in the absence of an avalanche process. Electrons tunnel from exchange-splitted localized states in the accumulation layer (Figure 25). If the tunneling transparency from the highest sublevel is greater than the transparency from lower sublevels, then the spin injection reaches high values. Magnetoresistive sensors are based on the IMR effect in $SiO_2$(Co)/GaAs heterostructures, which is observed at high voltages above the threshold of the avalanche process. The developing impact ionization produces holes, which move and are accumulated in the region of the potential barrier. Formed positive feedback leads to great changes in the flowing current. But this process has some deficiencies. (1) The IMR effect in $SiO_2$(Co)/GaAs heterostructures has the temperature-peak type character. (2) This effect is observed in heterostructures with semi-insulating GaAs and in heterostructures with $n$-GaAs of high resistivity.

It is very important to extend the IMR effect observed in $SiO_2$(Co)/GaAs heterostructures to heterostructures with other SCs and to reach the *IMR* coefficient of high values in a broad temperature range. One of the promising semiconductor for spintronics with enhanced lifetime and transport length is silicon, Si [42, 12, 43]. Spin-orbit effects producing spin relaxation are much smaller in Si than in GaAs owing to the lower atomic mass and the inversion symmetry of the crystal structure maintaining spin-degenerate bands. Furthermore, the most abundant isotope $^{28}$Si has no nuclear spin, suppressing hyperfine interactions. These properties make relatively long spin lifetimes in Si.

Considering the IMR effect in $SiO_2$(Co)/GaAs heterostructures, we can result in conclusion that for the efficient magnetoresistance in FM / SC heterostructures it is need to fulfill the following requirements.

(1) The SC contains a quantum well at the interface.

(2) The quantum well must contain localized electron levels.

(3) Localized levels must be exchange-splitted by the FM. Interaction with elec-

trons on these levels forms the spin-dependent barrier.
(4) Giant magnetoresistance effect can be achieved in the presence of the impact ionization process.
(5) The trap for holes produced by the impact ionization must be placed in the region of the potential barrier. Holes lower the barrier height. This forms the positive feedback and results in great changes in the current.

The studied $SiO_2$(Co)/GaAs heterostructures contain quantum wells formed by the $SiO_2$(Co) film due to the difference of the chemical potentials between the $SiO_2$(Co) and the GaAs. Width and form of these quantum wells are strongly dependent on the electron concentration at the interface and, therefore, on temperature. Using another methods to form quantum wells at interfaces in SCs (molecular beam epitaxy, MOCVD), we can obtain quantum wells with desired width, depth and number of localized electron levels. Magnetoresistive sensors with use the impact ionization process can be constructed on the basis of heterostructures with hole traps and quantum wells near the interface (Figure 29). Localized levels can be splitted by the exchange interaction with a FM grown at the interface or by the interaction with a granular film containing FM nanoparticles. It is need to note that the latter technology method – sputtering of the granular film can solve the problem of the efficient spin injection difficulty due to the inherent conductivity mismatch between FM metals and SCs [44]. Variation of the FM nanoparticle concentration leads to considerable variation in the conductivity of the granular film and we can reach conductivity correspondence between the FM and the SC. The additional barrier formed near the quantum well in the region of the hole trap makes possible to improve the onset of the impact ionization. Applied voltage drops on the barrier and, thus, forms high electrical field in this region sufficient to start the avalanche process.

It can be expected that the proposed magnetoresistive sensor possesses the magnetoresistive effect of high values in a broad temperature range. The quantum well has fixed width and depth. This leads to a fixed number of localized levels, which are responsible for the formation of the spin-dependent barrier. The number of levels is slightly dependent on temperature. There is the reason to believe that the magnetoresistive sensor based on this heterostructure can operate at a broader temperature range in comparison with sensors based on $SiO_2$(Co)/GaAs heterostructures, in which the quantum well at the interface is formed by the difference of chemical potentials of the GaAs and the granular film.

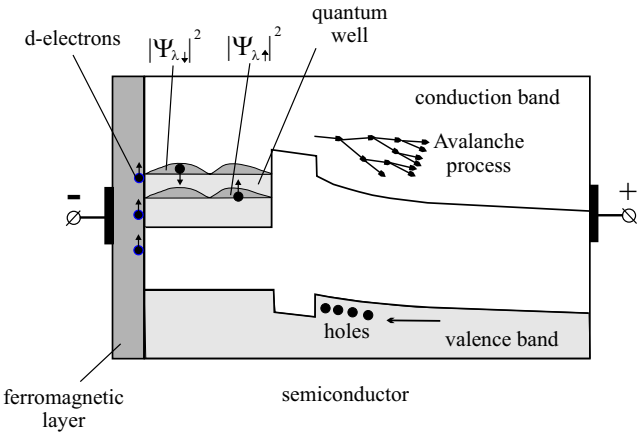


Figure 29. Schematic band diagram of the magnetoresistive sensor on the base of the heterostructure with quantum well and hole trap in the avalanche regime.

## Conclusion

The giant injection magnetoresistance (IMR effect) observed in $SiO_2$(Co)/GaAs heterostructures reaches high values. The IMR effect has positive values and is of the temperature-peak type character. The temperature location of the effect depends on the Co concentration and can be shifted by the applied electrical field. For the $SiO_2$(Co)/GaAs heterostructure with 71 at.% Co the IMR value reaches 1000 ($10^5$ %) at room temperature, which is two-three orders higher than maximum values of GMR in metal magnetic multilayers and TMR in magnetic tunnel junctions. On the contrary, for $SiO_2$(Co)/Si heterostructures magnetoresistance values are very small ($4\%$) and for $SiO_2$(Co) films the intrinsic magnetoresistance is equal to opposite values.

High values of the magnetoresistance effect in $SiO_2$(Co)/GaAs heterostructures have been explained by magnetic-field-controlled onset of the impact ionization and by the electron accumulation in the quantum well in the semiconductor interface region induced by the backscattering process of injected electrons on exchange-splitted levels. The spin-dependent potential barrier is formed in the accumulation electron layer in the semiconductor near the interface. The impact ionization induced by injected electrons produces holes, which move and are accumulated in the region of the potential barrier. Due to the formed

hole positive feedback small variations in the barrier height give great changes in the current. The applied magnetic field increases the height and reduces the transparency of the barrier. This suppresses the onset of the impact ionization and changes the potential distribution. The developed model can explain some features of experimental results. The spin-dependent potential barrier is due to the exchange interaction between electrons in the accumulation electron layer in the SC and $d$-electrons of Co. Existence of localized electron states in the accumulation layer results in high values of the barrier in the $SiO_2$(Co)/GaAs. This leads to the temperature-peak type character of the IMR. Maximum of the temperature IMR peak corresponds to a single exchange-splitted level in the accumulation layer. The temperature peak width is inversely proportional to the surface probability of the Co particle distribution at the interface. In contrast, for $SiO_2$(Co)/Si heterostructures the accumulation layer has small thickness without any localized states, is tunnel transparent and does not influence on the injection current.

Ferromagnetic / semiconductor heterostructures with quantum wells containing spin-polarized localized electrons in the semiconductor at the interface are proposed as efficient room-temperature spin injectors. In the avalanche regime heterostructures with holes traps and spin-dependent potential barrier in quantum wells can be used as efficient magnetic sensors.

### Acknowledgment

This work was supported by the Russian Foundation for Basic Research (Project No. 15-02-06208).

## References

[1] Lenz J. and Edelstein A.S., *IEEE Sensors Journal* **6**, 631 (2006).

[2] Ripka P. and Tipek A., *Modern sensors. Handbook*, Wiley, 2007.

[3] *Magnetic Sensors - Principles and Applications*, Ed. by Kevin Kuang, InTech, 2012, ISBN 978-953-51-0232-8.

[4] Lutsev L.V., Stognij A.I., and Novitskii N.N., *JETP Letters* **81**(10), 514 (2005).

[5] Lutsev L.V., *J. Phys.: Condens. Matter* **18**(26), 5881 (2006).

[6] Lutsev L.V., Stognij A.I., Novitskii N.N., and Stashkevich A.A., *J. Magn. Magn. Mater.* **300**, e12 (2006).

[7] Lutsev L.V., Stognij A.I., and Novitskii N.N., *Phys. Rev. B* **80**(18), 184423 (2009).

[8] Leonid Lutsev, *Giant injection magnetoresistance. Experimental and theoretical research, perspective applications.* Lambert Academic Publishing, Saarbrucken, Germany, 2013, ISBN 978-3-659-43964-3, [in Russian].

[9] Nordling J., Millen R.L., Bullen H.A., Porter M.D., Tondra M., and Granger M.C., *Anal. Chem.* **80**, 7930 (2008).

[10] Millen R.L., Nordling J., Bullen H.A., Porter M.D., Tondra M., and Granger M.C., *Anal. Chem.* **80**, 7940 (2008).

[11] Appelbaum I., Russel K.J., Monsma D.J., Narayanamurti V., Marcus C.M., Hanson M.P., and Gossard A.C., *Applied Physics Letters* **83**, 4571 (2003).

[12] Appelbaum I. and Monsma D.J., *Applied Physics Letters* **90**, 262501 (2007).

[13] Russel K.J., Appelbaum I., Wei Yi, Monsma D.J., Capasso F., Marcus C.M., Narayanamurti V., Hanson M.P., and Gossard A.C., *Applied Physics Letters* **85**, 4502 (2004).

[14] Akinaga H., Mizuguchi M., Ono K., and Oshima M., *Applied Physics Letters* **76**(3), 357 (2000).

[15] Akinaga H., *Semicond. Sci. Technol.* **17**(4), 322 (2002).

[16] Yokoyama M., Ogawa T., Nazmul A.M., and Tanaka M., *J. Appl. Phys.* **99**(8), 08D502 (2006).

[17] Akinaga H., De Boeck J., Borghs G., Miyanishi S., Asamitsu A., Van Roy W., Tomioka Y., and Kuo L.H., *Applied Physics Letters* **72**(25), 3368 (1998).

[18] Stognij A.I., Novitskii N.N., and Stukalov O.M., *Tech. Phys. Lett.* **28**, 17 (2002).

[19] Stognij A.I., Novitskii N.N., and Stukalov O.M., *Tech. Phys. Lett.* **29**, 43 (2003).

[20] Zvonareva T.K., Lebedev V.M., Polanskaya T.A., Sharonova L.V., and Ivanov-Omskii V.I., *Semiconductors* **34**, 1094 (2000).

[21] Barzilai S., Goldstein Y., Balberg I., and Helman J.S., *Phys. Rev. B* **23**, 1809 (1981).

[22] Yakushiji K., Mitani S., Takanashi K., Ha J.-G., and Fujimori H., *J. Magn. Magn. Mater.* **212**, 75 (2000).

[23] Sankar S., Dender D., Borchers J.A., Smith D.J., Erwin R.W., Kline S.R., and Berkowitz A.E., *J. Magn. Magn. Mater.* **221**, 1 (2000).

[24] Lin A.L., Omelianovski E., and Bube R.H., *J. Appl. Phys.* **47**, 1852 (1976).

[25] Yu P.W., *Appl. Phys. Lett.* **44**, 330 (1984).

[26] Baibich M.N., Broto J.M., Fert A., Nguyen Van Dau F., Petroff F., Eitenne P., Creuzet G., Friederich A., and Chazelas J., *Phys. Rev. Lett.* **61**, 2472 (1988).

[27] Binasch G., Grunberg P., Saurenbach F., and Zinn W., *Phys. Rev.* B **39**, 4828 (1988).

[28] Gijs M.A.M. and Bauer G.E.W., *Adv. Phys.* **46**, 285 (1997).

[29] Moodera J.S., Kinder L.R., Wong T.M., and Meservey R., *Phys. Rev. Lett.* **74**, 3273 (1995).

[30] Jiang X., Wang R., Shelby R., Macfarlane R.M., Bank S.R., Harris J.S., and Parkin S.S.P., *Phys. Rev. Lett.* **94**, 056601 (2005).

[31] Lee Y.M., Hayakawa J., Ikeda S., Matsukura F., and Ohno H., *Applied Physics Letters* **90**, 212507 (2007).

[32] Izyumov Yu.A., Kassan-ogly F.A., and Skryabin Yu.N., *Field Methods in the Theory of Ferromagnetism*, Nauka, Moscow, 1974.

[33] Abrikosov A.A., Gor'kov L.P., and Dzyaloshinski I.E., *Methods of Quantum Field Theory in Statistical Physics*, Dover, New York, 1975.

[34] Ruderman M.A. and Kittel C., *Phys. Rev.* **96**(1), 99 (1954).

[35] Kasuya T., *Prog. Theor. Phys.* **16**(1), 45 (1956).

[36] Yosida K., *Phys. Rev.* **106**(5), 893 (1957).

[37] Harrison W.A., *Electronic Structure and the Properties of Solids. The Physics of the Chemical Bond*, W.H. Freeman and Company, San Francisco, 1980.

[38] Davydov A.S., *Quantum Mechanics*, Pergamon Press, Oxford, 1976.

[39] Landau L.D. and Lifshitz E.M., *The Classical Theory of Fields*. Vol. 2 (4th ed), Butterworth-Heinemann, 1975.

[40] Fomenko V.S. and Podchernyaeva I.A., *Emission and Adsorption Properties of Substances and Materials*, Nauka, Moscow, 1975.

[41] *Handbook of Physical Quantities*, Ed. by Grigoriev I.S. and Meilikhov E.Z., CRC Press, Boca Raton, 1997.

[42] Jonker B.T., Kioseoglou G., Hanbicki A.T., Li C.H., and Thompson P.E., *Nature Physics* **3**, 542 (2007).

[43] Appelbaum I., Huang B., and Monsma D.J., *Nature* **447**, 295 (2007).

[44] Schmidt G., Ferrand D., Molenkamp L.W., Filip A.T., and van Wees B.J., *Phys. Rev. B* **62**(8), R4790 (2000).